UCRL- 91129
PREPRINT

SLIDING INTERFACES WITH CONTACT-IMPACT IN LARGE SCALE LAGRANGIAN COMPUTATIONS

J. O. Hallquist
G. L. Goudreau
D. J. Benson

This paper was prepared for submittal to The Third International Conference on Finite Elements in Nonlinear Mechanics (FENOMECH '84), Stuttgart, W. Germany, Sept. 10-14, 1984.

December, 1984

This is a preprint of a paper intended for publication in a journal or proceedings. Since changes may be made before publication, this preprint is made available with the understanding that it will not be cited or reproduced without the permission of the author.

VAULT REFERENCE COPY

Lawrence Livermore National Laboratory

DISCLAIMER

This document was prepared as an account of work sponsored by an agency of the United States Government. Neither the United States Government nor the University of California nor any of their employees, makes any warranty, express or implied, or assumes any legal liability or responsibility for the accuracy, completeness, or usefulness of any information, apparatus, product, or process disclosed, or represents that its use would not infringe privately owned rights. Reference herein to any specific commercial products, process, or service by trade name, trademark, manufacturer, or otherwise, does not necessarily constitute or imply its endorsement, recommendation, or favoring by the United States Government or the University of California. The views and opinions of authors expressed herein do not necessarily state or reflect those of the United States Government or the University of California, and shall not be used for advertising or product endorsement purposes.

LAWRENCE BERKELEY LABORATORY

SLIDING INTERFACES WITH CONTACT-IMPACT IN LARGE SCALE LAGRANGIAN COMPUTATIONS

J. O. Hallquist, G. L. Goudreau and D. J. Benson

University of California, Lawrence Livermore National Laboratory
P. O. Box 808, Livermore, California 94550 USA

ABSTRACT

The two and three dimensional contact algorithms used in the finite element programs developed at the Lawrence Livermore National Laboratory are described in this paper. We are interested in both static contact and dynamic impact problems and, consequently, have pursued the development of two different algorithms. The first, based on the hydrocode technology of the sixties, is implemented in our two and three dimensional explicit finite element codes. The second, a symmetric penalty treatment, is used in our implicit codes and is optional in the explicit codes. The penalty methods are used to obtain solutions to almost all of our structural problems but we find that the hydrocode approach is vastly superior if pressures greatly exceed the yield strength. Examples are provided to show practical applications of both approaches.

1. INTRODUCTION

The ability to treat structural problems where adjacent components may independently slide, separate, and impact along material interfaces is crucial in many varied technical fields. In weapons design, relevant problems include the structural response of gun fired projectiles,

laydown bombs, and a variety of shape charge designs of either the jet or fragment type. The nuclear industry analyzes the impact of shipping casks containing radioactive materials, pipe to pipe impact, and soil-structure interaction problems. Crashworthiness in the automotive and aircraft industry is another important area, as is biomechanics. The contact-impact capability has always been an important aspect of both the implicit and explicit finite element codes [1-4] developed at the Lawrence Livermore National Laboratory, where nearly all our applications depend on it. Our codes use well over 1000 CPU hours of LLNL Cray time per year, but considerably more would be used if it were available to the structural analysts. Our need for more analyses leads us to continually improve the speed and efficiency of the solution algorithms, relying to a large extent on ideas from the literature and our own research, including a considerable amount of numerical experimentation. Today, we can solve most two and three dimensional contact-impact, finite strain, plasticity problems of interest to us with almost complete confidence that no insurmountable numerical difficulties will arise.

The development of reliable implicit codes to do contact problems requires a sound global solution strategy. We have implemented modified Newton, full Newton, and quasi-Newton iteration schemes; the latter of which includes the BFGS [5] and Broyden's [6] methods. In our experience, the quasi-Newton line searches also contribute to the fast convergence of the modified and full Newton schemes. In three dimensions, we have ruled out full Newton as a viable option due to the extreme expense of reforming and factoring a large stiffness matrix for

each iteration. We now regularly use quasi-Newton methods with frequent reformations of the stiffness matrix. By optimally coding and fully vectorizing the stress divergence, the expense of equilibrium iterations including line search has been minimized.

Explicit hydrocodes use the viscosity method [7] to resolve the details of shock wave propagation through the mesh with small time step sizes dictated by the Courant stability limit. In three dimensions, our typical applications use 20000 elements, 10000 to 100000 time steps, with 20 to 30 percent of the nodal points contained in the contact surface definitions. Efficient, cheap algorithms are needed to make such problems affordable. We use primitive elements (one stress point hexahedrons), control the zero energy modes by the simpliest possible hourglass control [8], and have an efficient and reliable contact-impact algorithm. With faster and larger computers than presently available, we would quickly expand our three dimensional analyses to a point where the resolution is roughly equivalent to our two dimensional counterparts, i.e., by a factor of 10 to 50, therefore the need for efficient algorithms will continue for some time.

In developing general purpose contact algorithms for three dimensional solutions, we quickly realized that the rigorous extension of the two dimensional hydrocode algorithms though feasible, would be too costly. Our earlier experience has shown that Lagrange multiplier methods [9,10] did not necessarily preserve a smooth force distribution across interfaces. The lack of a smooth force field excited the zero energy modes in the primitive elements in nearly all the contact-impact problems we solved. Furthermore, these modes usually stopped explosive-

metal interaction computations, a major application for two dimensional hydrocodes, early in the solution. Thus, we were left with the penalty method as the method of choice. We now use the penalty approach in our two and three dimensional implicit and explicit codes, but, because it is not always suitable for applications involving high explosives, we retain an approach in our explicit codes that is based in part on the hydrocode methodology developed several decades ago.

In the development which follows, we shall first discuss the hydrocode slideline methodology developed in the 60's. Our DYNA2D algorithm, based on this work, has been extended to include impact and separation along the slideline. We also implemented this methodology in three dimensions but without the DYNA2D extensions. In Section 3, we discuss the penalty method. In the last section, we present a few applications.

2. HYDROCODE METHODOLOGY

In two dimensions, the contact surfaces along a slideline appear as lines in the yz plane where y is the horizontal axis, and z is the vertical axis and the axis of revolution in axisymmetric problems. These lines will be referred to as the master and slave lines respectively. Nodal points along the slave and master lines will be referred to as slave and master nodes, respectively. Likewise, line segments joining adjacent slave and master nodes will be called slave and master segments. Elements that have at least one side that is a slave segment are called slave elements, and master elements are similarly defined. Fig. 1 shows a typical interface. Slave nodes are constrained to slide on or close to the master line unless a tensile

interface force develops. In the early slideline algorithms discussed below, these lines were not allowed to separate. Designation of master and slave lines is required as input for the slideline definitions in most hydrocodes. A truly symmetric treatment such as used in our penalty algorithm would make this distinction irrelevant, but we are aware of no published treatments that are symmetric in the hydrocode literature.

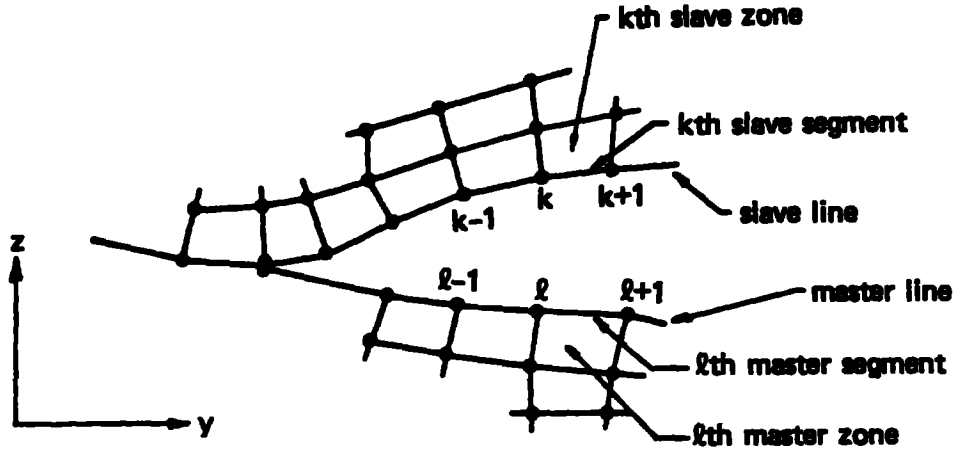

Fig. 1. Typical interface.

In the finite element computer implementation of the hydrocode algorithms, no changes to the explicit solution scheme are required since it is possible to organize the algorithm such that the logic external to the interface treatment applies to each node including the slave and master nodes. The additional subroutines are called once every time step following the calculation of the accelerations but prior to updating the velocity vector.

The definition of the slave and master lines is accomplished in DYNA2D by the user who provides a list of nodal point numbers of the

nodes lying on these lines. These numbers are given in the order they appear as one moves along the interface keeping the slave line on the left. Slave elements are identified in the initialization phase of DYNA2D by a search of the element connectivities and are ordered such that the first element corresponds to the first slave node, the second element to the second slave node, and so on.

In the sections which follow we will describe the algorithms of HEMP [11], TOODY [12], TENSOR [13], as well as our own more recent efforts in DYNA2D which is based on this earlier work.

2.1 HEMP Finite Difference Code

In 1964, Wilkins published the HEMP finite difference equations based on the integral difference method [14]. A logically regular mesh was used made from a grid of intersecting j and k lines with slidelines permitted along k lines. A weakly coupled slideline algorithm was given (the mass in the slave elements was ignored), but modifications were clearly outlined for incorporating strong coupling. The actual modifications were included in a later revision of the original document [15]. In Wilkins' approach, a pressure boundary condition is applied to each segment of the master surface based on the stress state in the slave elements across from the center of the master element containing the segment. The pressure, p_ℓ for the ℓth master segment is given by (see Fig. 2).

$$p_\ell = (1-\alpha)p_k + \alpha p_{k+1} \qquad (2.1)$$

where p_k and p_{k+1} are the normal stress components in slave elements k and k+1

$$p_k = -(\sigma_{yy}^k \sin^2\theta_{\ell,\ell+1} + \sigma_{zz}^k \cos^2\theta_{\ell,\ell+1} - \sigma_{yz}^k \sin 2\theta_{\ell,\ell+1})$$

$$p_{k+1} = -(\sigma_{yy}^{k+1} \sin^2\theta_{\ell,\ell+1} + \sigma_{zz}^{k+1} \cos^2\theta_{\ell,\ell+1} - \sigma_{yz}^{k+1} \sin 2\theta_{\ell,\ell+1}) \quad (2.2)$$

and $\theta_{\ell,\ell+1}$ is the included angle taken counterclockwise between the y-axis and the line from ℓ to $\ell+1$. The parameter α is a dimensionless distance

$$\alpha = \frac{L'}{L} \quad (2.3)$$

where L is the distance between the element centers of slave elements k and k+1 and L' is distance from the center of slave element k to the intersection of a line drawn from the center of the master element ℓ normal to segment ℓ with the line drawn between the slave element centers. After repeating this procedure for each master segment, the entire surface is accelerated as a free surface with a pressure boundary condition.

To attain the goal of a strongly coupled algorithm it is necessary to include the mass of the slave surface. A constant factor, z, is defined for the entire slideline and is used to scale the normal component of the acceleration.

$$z = \frac{\sum_{i=1}^{nm} M_i^m + \sum_{i=1}^{ns} M_i^s}{\sum_{i=1}^{nm} M_i^m} \quad (2.4)$$

In Eq. (2.4), nm and ns are the total number of master and slave elements along the slideline, and M_i^m and M_i^s are the total mass in the

ith master and slave elements respectively. The master node accelerations are rotated into the local coordinate system of the node and the normal acceleration is scaled to account for the added mass of the slave surface.

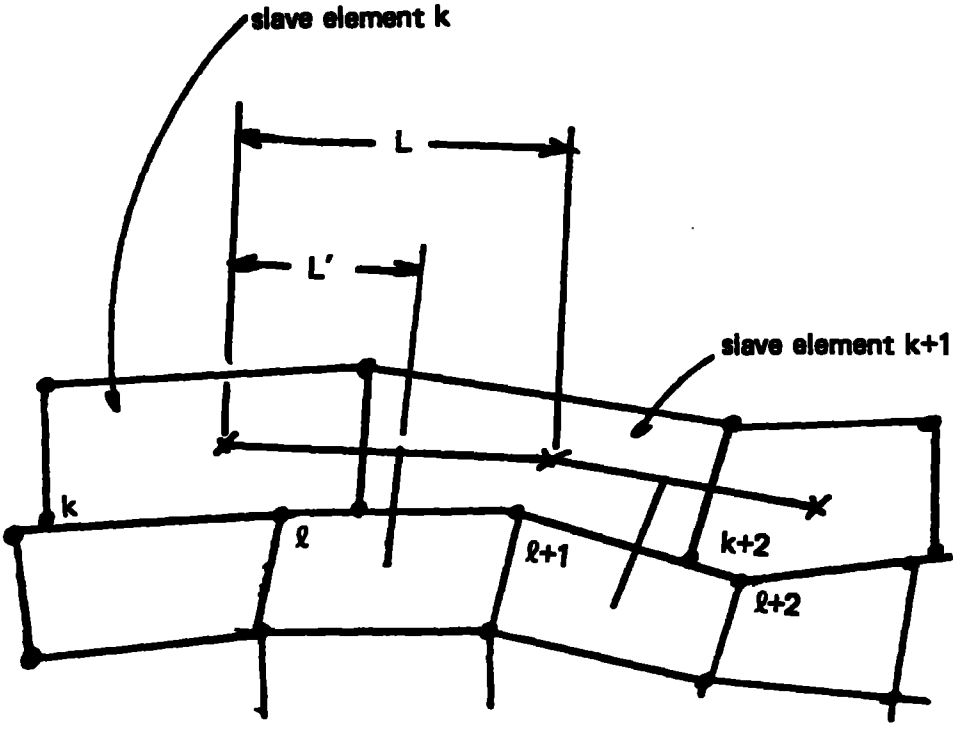

Fig. 2. Interpolation scheme to determine interface pressure (Wilkins [11]).

$$a_{n_\ell}^{n+1} = \frac{1}{z}\left(\ddot{z}_\ell^{+}\cos\theta_{\ell-1,\ell+1} - \ddot{y}_\ell^{+}\sin\theta_{\ell-1,\ell+1}\right) \tag{2.5a}$$

$$a_{t_\ell}^{n+1} = \ddot{y}_\ell^{+}\cos\theta_{\ell-1,\ell+1} + \ddot{z}_\ell^{+}\sin\theta_{\ell-1,\ell+1} \tag{2.5b}$$

In the local coordinate system, the normal direction at point ℓ is perpendicular to a line drawn from ℓ-1 to ℓ+1. The superscript, +, signifies that acceleration has been updated for the pressure distribution. The global accelerations are calculated by rotating the

scaled acceleration vector back to the global frame.

$$\tilde{y}_{\ell}^{n+1} = a_{t_{\ell}}^{n+1} \cos\theta_{\ell-1,\ell+1} - a_{n_{\ell}}^{n+1} \sin\theta_{\ell-1,\ell+1} \tag{2.6a}$$

$$\tilde{z}_{\ell}^{n+1} = a_{n_{\ell}}^{n+1} \cos\theta_{\ell-1,\ell+1} + a_{t_{\ell}}^{n+1} \sin\theta_{\ell-1,\ell+1} \tag{2.6b}$$

The final step is the update of the motion of the slave surface. Each slave node k is moved tangentially, treating the master surface as a symmetry plane in the configuration at time n. The slave nodes are projected back on to the master surface, after the surface is updated into the n+1 configuration, along the j line on the slave side that contains the kth slave node. Velocities for the slave nodes are then found by dividing the change in coordinates by the time step size.

$$\begin{aligned} \dot{y}^{n+1/2} &= (y^{n+1} - y^{n})/\Delta t^{n+1/2} \\ \dot{z}^{n+1/2} &= (z^{n+1} - z^{n})/\Delta t^{n+1/2} \end{aligned} \tag{2.7}$$

In early versions of HEMP, the constant z-factor of Eq. (2.4) was used rather than a spatially (j) dependent factor. Of course, the assumption of a constant mass distribution is not generally valid and this was acknowledged by Wilkins. Another approximation involved the computation of interface pressure from Eqs. (2.1) and (2.2) where only two slave elements in the immediate vicinity of the master segment are considered whereas a weighted average of all contiguous slave elements would give a more realistic representation of p_{ℓ}. Also, the pressure normal to the master segment defined by rotating the planar stress is

valid only in plane strain in constant Jacobian elements. Ignoring the geometry of the element and the effects of hoop stress on p_ℓ can lead to values that are too high or low. The methodology of TOODY and TENSOR discussed below overcomes these weaknesses.

2.2 TOODY Finite Difference

In the TOODY implementation of sliding interfaces, Bertholf and Benzley applied the integral difference method to each master node along the sliding interface. During each cycle a new mesh is defined overlaying the slave elements and matching the mesh density of the contiguous master surface. We shall briefly outline our implementation of the TOODY algorithm in DYNA2D.

First we must locate the coordinates of element k*, where the asterisk superscript denotes phony elements and related variables that are assumed to lie in the slave elements that overlap the master nodes. The position of point j* in Fig. 3, for example, is determined such that the ratio of the distances is constant when $d_{k,\ell}$ is the distance from point k to ℓ.

$$\frac{d_{k,\ell}}{d_{k,k+1}} = \frac{d_{j,j^*}}{d_{j,j+1}} \tag{2.8}$$

The stresses in the newly defined slave elements are based on a length weighted interpolation along the master surface. Consider Fig. 3 where slave element k is the first element to overlap master segment ℓ and underlie the phony element k*. Letting S_ℓ denote the length of the master segment ℓ, n_ℓ denote the unit vector tangent to segment ℓ, and $\underset{\sim}{r}_{\ell,k}$ denote the vector drawn from ℓ to slave node k, we can define $S_{\ell,k}$ for each slave node.

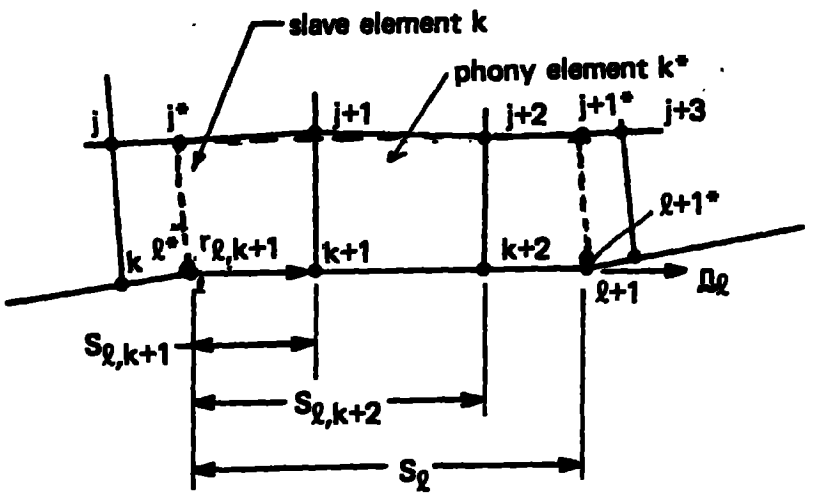

Fig. 3. A typical master segment where slave elements k, k+1, and k+2 contribute to the pressure load applied to master segment ℓ. Phony element k* is indicated by dashed lines.

$$S_{\ell,k} = \underset{\sim}{r}_{\ell,k} \cdot \underset{\sim}{n}_\ell \quad \text{if} \quad \underset{\sim}{r}_{\ell,k} \cdot \underset{\sim}{n}_\ell > 0 \tag{2.9a}$$

$$S_{\ell,k} = 0 \quad \text{if} \quad \underset{\sim}{r}_{\ell,k} \cdot \underset{\sim}{n}_\ell \leq 0 \tag{2.9b}$$

$$S_{\ell,k+1} = \underset{\sim}{r}_{\ell,k+1} \cdot \underset{\sim}{n}_\ell \quad \text{if} \quad \underset{\sim}{r}_{\ell,k+1} \cdot \underset{\sim}{n}_\ell < S_\ell \tag{2.9c}$$

$$S_{\ell,k+1} = S_\ell \quad \text{if} \quad \underset{\sim}{r}_{\ell,k+1} \cdot \underset{\sim}{n}_\ell \geq S_\ell \tag{2.9d}$$

The stress contribution to slave element k* made by the stress in slave element k, σ^k_{ij}, is designated $\sigma^{k*}_{ij,k}$ and defined by Eq. (2.10).

$$\sigma^{k*}_{ij,k} = (S_{\ell,k+1} - S_{\ell,k})\ \sigma^k_{ij} / S_\ell \tag{2.10}$$

If inequality Eq. (2.9d) is satisfied, $\sigma^{k*}_{ij,k}$ determines the stress in phony element k*; otherwise, the contribution to the stress tensor of the next overlapped slave element is added. For example, consider the contribution of zone k+1 to the phony k* zone.

$$S_{\ell,k+2} = \underset{\sim}{r}_{\ell,k+2} \cdot \underset{\sim}{n}_{\ell} \quad \text{if} \quad \underset{\sim}{r}_{\ell,k+2} \cdot \underset{\sim}{n}_{\ell} < S_{\ell} \tag{2.11a}$$

$$S_{\ell,k+2} = S_{\ell} \quad \text{if} \quad \underset{\sim}{r}_{\ell,k+2} \cdot \underset{\sim}{n}_{\ell} \geq S_{\ell} \tag{2.11b}$$

$$\sigma^{k*}_{ij,k+1} = (S_{\ell,k+2} - S_{\ell,k+1})\, \sigma^{k+1}_{ij} / S_{\ell} \tag{2.12}$$

If Eq. (2.11b) is unsatisfied, k again is incremented by 1, and the procedure is given by Eqs. (2.11)-(2.12) continues until Eq. (2.11b) is satisfied. The stress tensor for k* becomes

$$\sigma^{k*}_{ij} = \sum_{i=0}^{n-1} \sigma^{k*}_{ij,k+i} \tag{2.13}$$

where n is the number of overlapping elements. After repeating this procedure to determine the bulk viscosity q^{k*} and density ρ^{k*}, we proceed to the next phony element, k+1*, and repeat the procedure.

We enter the slideline logic in DYNA2D after computing the nodal forces, and therefore the free surface accelerations of the slave and master nodes are available by dividing the nodal forces by the nodal masses. The tangential accelerations of the master nodes are calculated as if they are free surface nodes, by using Eq. (2.5b). For the normal acceleration, the master node is temporarily treated as an interior node surrounded by the master elements and the phony slave elements. A new acceleration $(\ddot{y}^{+}_{\ell}, \ddot{z}^{+}_{\ell})$ is computed, and substituted into Eq. (2.5a) with z=1. The modified global acceleration is calculated from $a^{n+1}_{t_{\ell}}$ and $a^{n+1}_{n_{\ell}}$ by using Eq. (2.6).

In the update of the slave surface motion, Bertholf and Benzley projected the slave nodes normally on to the updated master surface and moved them tangentially according to their tangential velocities and accelerations. This is illustrated in Fig. 4.

$$\Delta x_{t_k}^{n+1} = (v_{t_k}^{n+\frac{1}{2}} + a_{t_k}^{n} \Delta t^{n}) \Delta t^{n+\frac{1}{2}} \qquad (2.14)$$

Using the configurations at n and n+1 the slave node velocities are then computed from Eq. (2.7).

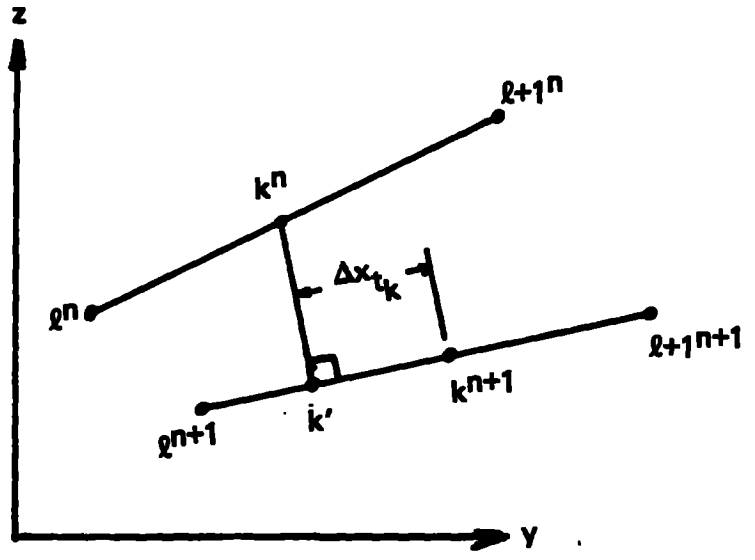

Fig. 4. Update of the position of slave node k from time n to n+1 given by Bertholf and Benzley [12].

2.3 TENSOR Finite Difference Code

Of the hydrocode treatments discussed in this paper, the TENSOR contact-impact algorithm comes closest to being symmetric. Like the approach in TOODY, phony elements are defined that overlay the slave elements and have interpolated values of stresses and densities. Phony slave nodes are created at each master node and are assigned velocities that are interpolated from the actual slave nodes. Consider master node

ℓ and phony node ℓ^* as shown in Fig. 3. From rigid body dynamics we can treat ℓ^* as a particle that has a zero normal velocity relative to a rotating coordinate system with its origin at node ℓ and write the constraint equation for the normal acceleration.

$$a_{n_{\ell^*}} = a_{n_\ell} + a_c \tag{2.15}$$

$$a_c = 2\omega_\ell \left[(\dot{y}_{\ell^*}-\dot{y}_\ell)\cos\theta_{\ell-1,\ell+1} + (\dot{z}_{\ell^*}-\dot{z}_\ell)\sin\theta_{\ell-1,\ell+1}\right]$$

The normal direction at node ℓ is perpendicular to a line drawn from nodes ℓ-1 to ℓ+1, a_c is the Coriolis acceleration term, and ω_ℓ is the angular velocity at node ℓ.

$$\omega_\ell = \frac{(\dot{z}_{\ell+1}-\dot{z}_{\ell-1})\cos\theta_{\ell-1,\ell+1} - (\dot{y}_{\ell+1}-\dot{y}_{\ell-1})\sin\theta_{\ell-1,\ell+1}}{d_{\ell-1,\ell+1}} \tag{2.16}$$

The expressions for the normal accelerations in terms of an interface pressure p with Eqs. (2.15) and (2.16) are solved for p.

$$a_{n_\ell} = (f_{n_\ell} - \tfrac{p}{2} c_\ell) / m_\ell \tag{2.17a}$$

$$a_{n_{\ell^*}} = (f_{n_{\ell^*}} + \tfrac{p}{2} c_\ell) / m_{\ell^*} \tag{2.17b}$$

$$c_\ell = (z_{\ell+1}-z_{\ell-1})\sin\theta_{\ell-1,\ell+1} + (y_{\ell+1}-y_{\ell-1})\cos\theta_{\ell-1,\ell+1} \tag{2.18}$$

Here, M_ℓ and M_{ℓ^*} are the lumped masses, and f_{n_ℓ} and $f_{n_{\ell^*}}$ are the normal components of the nodal forces at nodes ℓ and ℓ^* due to the internal stress states.

Eq. (2.17a) permits the normal acceleration of the master surface to be updated. This procedure is repeated for each master node. Since the tangential component of the acceleration is unchanged, the global components can be found from Eq. (2.6).

Unlike the HEMP and TOODY schemes, where the slave node is moved with the master surface, the TENSOR scheme repeats the foregoing process creating phony nodes and elements on the master side to accelerate the slave surface. After the geometry is updated, slave nodes that do not lie on the master surface are projected normally to the surface. Normal components of velocity are then reset by interpolating from the master side.

2.4 DYNA2D Finite Element Code

The implementation in DYNA2D will be discussed in detail. Ideas from HEMP, TOODY, and TENSOR underlie the current DYNA2D algorithm. Although we feel that the TENSOR scheme may be superior on some problems, it is considerably more expensive and is not easily extended to handle impact problems.

Our current interface treatment may be outlined as follows:

1. Update the location of each slave node by identifying its closest master node if it is not in contact with the master surface or by identifying the first master node of the master segment on which it lies.
2. For each master segment, identify the first overlapping slave element.
3. Check each slave node that lies in contact with the master surface for the existence of a tensile interface force, and if the force is tensile, release it.

4. Distribute one-half the mass of each slave element to the appropriate master nodes if both slave nodes of the slave segment associated with the element are in contact. If neither of these slave nodes are in contact, distribute no mass. If one slave node is in contact, distribute one-half the mass lying between the contacting node and the center of the slave segment of the slave element.
5. Whenever a slave node reaches the master surface, apply the interface conditions to determine the post-impact velocity.
6. From the states of stress in the slave elements, compute a distributed pressure for each master segment and the equivalent nodal forces. A slave element must be in contact with the master surface to contribute force.
7. For each slave node in contact with a master segment, compute its tangential velocity and acceleration. Interpolate the normal components of velocity and acceleration from the adjacent master nodes.
8. For slave nodes not in contact with the master surface check for penetration during the next time step and reduce the time step size if necessary so that no slave node penetrates.

The above steps are explained below in more detail. A typical interface is considered that is assumed to consist of n_s slave nodes, n_s-1 slave elements, and n_m master nodes. An assumption is made that the master line is sufficiently long so that slave nodes in contact with the line will not slide off the end of the line. In practice, master line extensions are used to ensure that this is the case or, if the user

prefers, the slave nodes that slide off can be treated as free surface nodes. If more than one interface exists, the procedures outlined here are repeated for each interface.

2.4.1 Slave node search

Consider slave node k ($1 < k < n_s$) and assume that a search of the master line has located the master node ℓ ($1 < \ell < n_m$) lying closest to k. If k is free, the next slave node is considered. If k is sliding on the master surface, the master segment that contains k must be determined. Fig. 5 depicts a portion of the master surface where slave node k and master node ℓ are labeled. Node k lies on the segment bounded by ℓ-1 and ℓ, called master segment ℓ-1, if

$$\underset{\sim}{r}_{\ell-1,\ell+1} \cdot \underset{\sim}{r}_{\ell,k} \leq 0 \tag{2.19}$$

or on the segment bounded by ℓ and ℓ+1, called master segment ℓ, if

$$\underset{\sim}{r}_{\ell-1,\ell+1} \cdot \underset{\sim}{r}_{\ell,k} > 0 \tag{2.20}$$

where $\underset{\sim}{r}_{\ell-1,\ell+1}$ is the vector from ℓ-1 to ℓ+1, and, likewise, $\underset{\sim}{r}_{\ell,k}$ is the vector from ℓ to k.

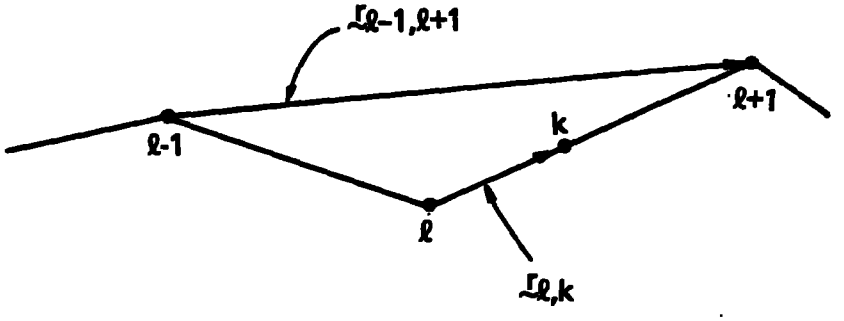

Fig. 5. Given that slave node k lies closest to master node ℓ, the sign of the dot product of vectors $\underset{\sim}{r}_{\ell,k}$ and $\underset{\sim}{r}_{\ell-1,\ell+1}$ determines the master segment that contains k.

2.4.2 Slave element search

This search identifies the first slave element to overlap each master segment. Pressure contributions are made by all slave elements that overlap the segment beginning with the element identified here and ending with the last element that overlaps the segment. In Fig. 6, a portion of the master line is shown in contact with the slave line.

Consider master segment ℓ . Recall that $\underset{\sim}{n}_{\ell}$ is the unit vector tangent to master segment ℓ and let k ($1 \leq k < n_s$) be the closest slave node to master node ℓ. Slave element k is identified as the first slave element to overlap master segment ℓ if any of the following tests are satisfied:

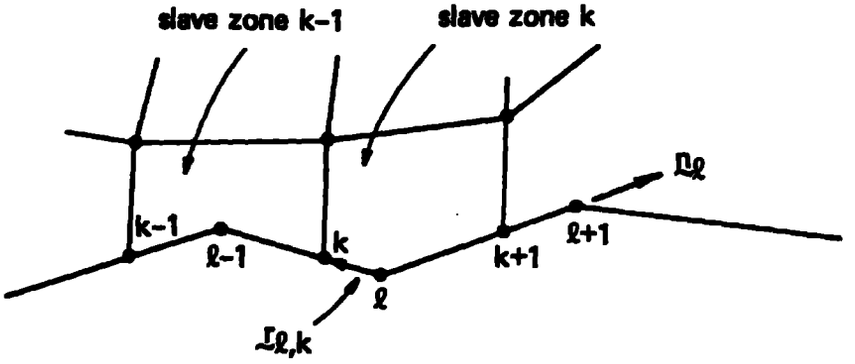

Fig. 6. A typical portion of the master line which shows slave element k as the first element to overlap master segment ℓ.

$$\underset{\sim}{r}_{\ell,k} \cdot \underset{\sim}{n}_{\ell} \leq 0 \qquad \text{for } 1 \leq k < n_s - 1 \qquad (2.21a)$$

$$\left.\begin{aligned} &\underset{\sim}{r}_{\ell,k} \cdot \underset{\sim}{n}_{\ell} \leq 0 \\ &\underset{\sim}{r}_{\ell,k+1} \cdot \underset{\sim}{n}_{\ell} > 0 \end{aligned}\right\} \quad \text{for } k = n_s - 1 \qquad (2.21b)$$

$$\left.\begin{aligned} &\underset{\sim}{r}_{\ell,k} \cdot \underset{\sim}{n}_{\ell} > 0 \\ &\underset{\sim}{r}_{\ell+1,k} \cdot \underset{\sim}{n}_{\ell} < 0 \end{aligned}\right\} \quad \text{for } k = 1 \qquad (2.21c)$$

If not, slave element k-1 is identified as the first overlapping element if

$$\underset{\sim}{r}_{\ell,k-1} \cdot \underset{\sim}{n}_{\ell} < 0 \qquad \text{for } 1 < k < n_s - 1 \qquad (2.22a)$$

$$\left.\begin{aligned} &\underset{\sim}{r}_{\ell,k} \cdot \underset{\sim}{n}_{\ell} > 0 \\ &\underset{\sim}{r}_{\ell,k-1} \cdot \underset{\sim}{n}_{\ell} < 0 \end{aligned}\right\} \quad \text{for } k = n_s - 1 \qquad (2.22b)$$

If the test given by Eqs. (2.21) and (2.22) fail, then no slave element overlaps the master segment being considered.

2.4.3 Tensile interface force

Consider slave node k and assume that it lies in contact with master segment ℓ. If the normal acceleration of the slave node relative to the master segment is positive, a tensile force is indicated, and the slave node is set free.

The normal acceleration of node k relative to segment ℓ is $\Delta\bar{\bar{a}}_{n_{k\ell}}$, which is defined by Eq. (2.23).

$$\Delta\ddot{\underline{a}}_{k\ell} = \ddot{\underline{a}}_{n_k} - (1 - \alpha_k)\, \ddot{\underline{a}}_{n_\ell} - \alpha_k\, \ddot{\underline{a}}_{n_{\ell+1}} \tag{2.23}$$

The local coordinate α_k is defined by Eq. (2.24).

$$\alpha_k = \underset{\sim}{n}_\ell \cdot \underset{\sim}{r}_{\ell k} \;/\; (\underset{\sim}{n}_\ell \cdot \underset{\sim}{r}_{\ell,\ell+1}) \tag{2.24}$$

If $\alpha_k < \varepsilon$ or if $\alpha_k > 1-\varepsilon$, where ε is a tolerance typically in the range of .005, the angle $\theta_{\ell-1,\ell+1}$ or $\theta_{\ell,\ell+2}$ is used in place $\theta_{\ell,\ell+1}$ determine the normal in Eq. (2.23). The right superscript, -, on nodal quantities denotes the values of the quantities before interface coupling is taken into account.

2.4.4 Addition of slave mass to master mass

The mass of the slave elements along the master surface is attributed to the appropriate master nodes. Each slave element is considered separately.

Consider the kth slave element. The mass to be distributed is given by

$$m_k = \frac{1}{2}\, \rho_k\, A_k \tag{2.25}$$

for plane strain. For axisymmetric problems, the DYNA2D Petrov-Galerkin scheme is used and, in the above equations, ρ_k and A_k are the density and area of the kth slave element in the current configuration.

As indicated previously, the kth slave element corresponds to the kth slave node. The kth slave node is being tracked by the master node ℓ and is, therefore, known to lie on master segment ℓ bounded by master nodes ℓ and $\ell+1$. Let

$$L_{k,\ell} = \underset{\sim}{s}_{k,\ell} \cdot \underset{\sim}{n}_k \qquad \text{if} \quad \underset{\sim}{s}_{k,\ell} \cdot \underset{\sim}{n}_k > 0$$

$$L_{k,\ell} = 0 \qquad \text{if} \quad \underset{\sim}{s}_{k,\ell} \cdot \underset{\sim}{n}_k \leq 0 \tag{2.26}$$

where $\underset{\sim}{s}_{k,\ell}$ is the vector from the kth slave node to the center of master segment ℓ and $\underset{\sim}{n}_k$ is the unit vector tangent to the slave segment k bounded by slave nodes k and k+1.

$$\underset{\sim}{n}_k = \underset{\sim}{r}_{k,k+1} / |\underset{\sim}{r}_{k,k+1}| \tag{2.27}$$

Let L_k denote the length of slave segment k: i.e., $L_k = \underset{\sim}{n}_k \cdot \underset{\sim}{r}_{k,k+1}$. The mass attributed to master node ℓ from slave element k, $m_{k,\ell}$, is given by Eq. (2.28).

$$m_{k,\ell} = (L_{k,\ell} / L_k) m_k \qquad \text{if} \quad L_k > L_{k,\ell} \tag{2.28a}$$

or

$$m_{k,\ell} = m_k \qquad \text{if} \quad L_k \leq L_{k,\ell} \tag{2.28b}$$

If inequality (2.28b) is satisfied, the next slave element is considered; otherwise, let

$$L_{k,\ell+1} = \underset{\sim}{s}_{k,\ell+1} \cdot \underset{\sim}{n}_k \qquad \text{if} \quad \underset{\sim}{s}_{k,\ell+1} \cdot \underset{\sim}{n}_k < L_k \tag{2.29a}$$

$$L_{k,\ell+1} = L_k \qquad \text{if} \quad \underset{\sim}{s}_{k,\ell+1} \cdot \underset{\sim}{n}_k \geq L_k \tag{2.29b}$$

where $\underset{\sim}{s}_{k,\ell+1}$ is the vector from the kth slave node to the center of master segment ℓ+1. The mass attributed to master node ℓ+1 from slave element k is given by Eq. (2.30).

$$m_{k,\ell+1} = \frac{L_{k,\ell+1} - L_{k,\ell}}{L_k} m_k \tag{2.30}$$

If Eq. (2.29b) is satisfied, the next slave element is considered; otherwise, the above procedure, using Eqs. (2.29) and (2.30) with subscript ℓ increased by one is repeated until Eq. (2.29b) is satisfied. This procedure is illustrated in Fig. 7.

The foregoing procedure is modified slightly whenever a void exists between the master surface and the kth element. If neither slave node lies on the master surface, the next slave element is immediately considered. If only one slave node is in contact, L_k is set to one-half of the length of slave segment, and, if node k is in contact, no other changes are required. If node k+1 is in contact, vector $\underset{\sim}{s}_{k,\ell+i}$ (i=1,2,...) is computed with its origin at the center of the slave segment.

2.4.5 Momentum calculations

Assume slave node k impacts the master line. By conserving momentum, the post-impact velocity of the master line can be obtained. The amount of mass associated with slave node k is taken as one-half of the mass included from the center of slave segment k-1 of slave element k-1 to the center of slave segment k of slave element k. Let $m^+_{k,\ell}$ denote the mass associated with slave node k that is attributed to master node ℓ. The mass that is distributed as described above includes $m^+_{k,\ell}$. The momentum calculation is made to determine the normal velocity of master node ℓ where the summation is performed over all of the slave nodes contributing to the mass of master node ℓ.

$$v^+_{n_\ell} = [(M^+_\ell - m^+_{k,\ell})\, v^-_{n_\ell} + m^+_{k,\ell}\, v^-_{n_k}] \,/\, M^+_\ell \qquad (2.31)$$

$$M_{\ell}^{+} = \sum_{i} m_{i,\ell} + M_{\ell} = \Delta M_{\ell} + M_{\ell} \tag{2.32}$$

M_{ℓ} is the mass at node ℓ, $v_{n\ell}^{-}$ and v_{nk}^{-} are the pre-impact velocities of master node ℓ and slave node k, respectively.

$$\begin{aligned} v_{n_{\ell}}^{-} &= \dot{z}_{\ell}^{-} \cos\theta_{\ell-1,\ell+1} - \dot{y}_{\ell}^{-} \sin\theta_{\ell-1,\ell+1} \\ v_{n_{k}}^{-} &= \dot{z}_{k}^{-} \cos\theta_{\ell-1,\ell+1} - \dot{y}_{k}^{-} \sin\theta_{\ell-1,\ell+1} \end{aligned} \tag{2.33}$$

Defining the tangential component of the velocity with Eq. (2.34), the global post-impact velocities of ℓ are given by Eq. (2.35)

$$v_{t_{\ell}}^{-} = \dot{y}_{\ell}^{-} \cos\theta_{\ell-1,\ell+1} + \dot{z}_{\ell}^{-} \sin\theta_{\ell-1,\ell+1} \tag{2.34}$$

$$\begin{aligned} \dot{y}_{\ell}^{+} &= v_{t_{\ell}}^{-} \cos\theta_{\ell-1,\ell+1} - v_{n_{\ell}}^{+} \sin\theta_{\ell-1,\ell+1} \\ \dot{z}_{\ell}^{+} &= v_{n_{\ell}}^{+} \cos\theta_{\ell-1,\ell+1} - v_{t_{\ell}}^{-} \sin\theta_{\ell-1,\ell+1} \end{aligned} \tag{2.35}$$

2.4.6 Master surface force distribution

The pressure acting on a master surface segment is interpolated from the slave elements in contact with the segment. This is accomplished with identical procedures as used to interpolate stresses for the phony elements in the TOODY scheme; therefore,

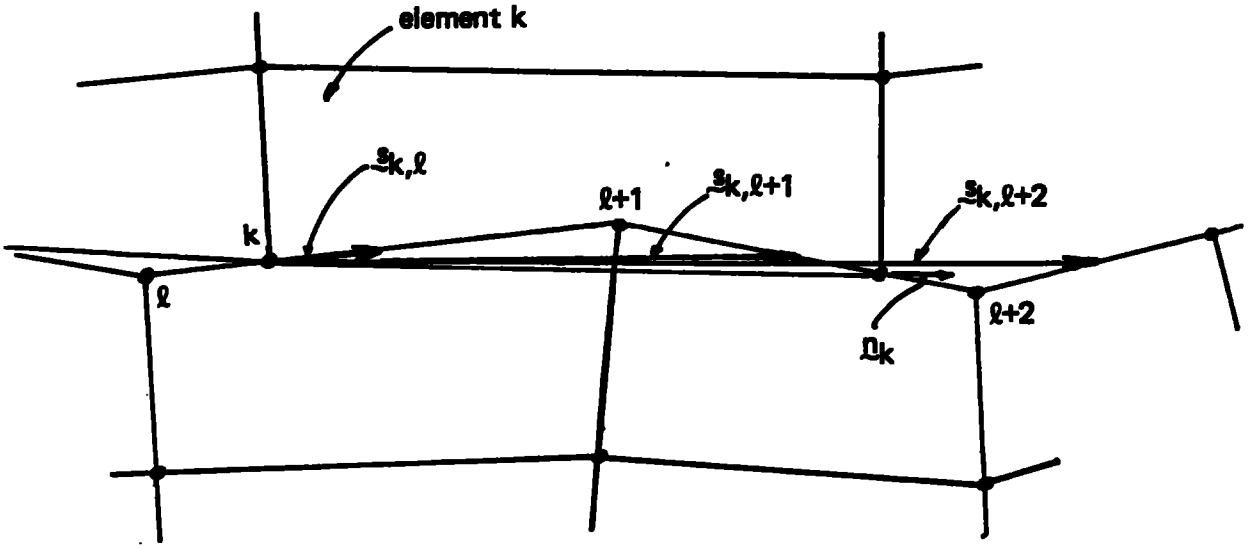

$$m_{k,\ell} = \frac{L_{k,\ell}}{L_k} m_k = \frac{s_{k,\ell} \cdot n_k}{L_k} m_k$$

$$m_{k,\ell+1} = \frac{L_{k,\ell+1} - L_{k,\ell}}{L_k} m_k$$

$$m_{k,\ell+2} = \frac{L_{k,\ell+2} - L_{k,\ell+1}}{L_k} m_k = \frac{L_k - L_{k,\ell+1}}{L_k} m_k$$

Fig. 7. Distribution of slave mass to master surface. In the case illustrated element k distributes mass to master nodes ℓ, ℓ+1, and ℓ+2.

Eqs. (2.9)-(2.13) apply here as well. However, rather than needing to interpolate the entire stress tensor, bulk q, and density, we need only interpolate the pressure distribution that equilibrates the normal components of force along the slideline.

With reference to Fig. 3, the contribution of pressure to master segment ℓ made by slave element k is designated by $p_{\ell,k}$ and defined by Eq. (2.36), where σ_{ℓ}^{k} is the effective stress in slave element k perpendicular to master segment ℓ.

$$p_{\ell,k} = (S_{\ell,k+1} - S_{\ell,k})\ \sigma_{\ell}^{k} / S_{\ell} \tag{2.36}$$

$$\sigma_{\ell}^{k} = \frac{f_{n_k} + f_{n_{k+1}}}{L_k} \tag{2.37}$$

We can determine the normal forces with Eq. (2.38), where f_{y_k}, f_{z_k}, $f_{y_{k+1}}$ and $f_{z_{k+1}}$ are components of $\underset{\sim}{f}_k$ defined by the integral in Eq. (2.39) of the transpose of the strain displacement matrix $\underset{\sim}{B}$ multiplied by the element stress vector $\underset{\sim}{\sigma}$ over the current geometry.

$$\begin{aligned} f_{n_k} &= f_{z_k} \cos\theta_{\ell,\ell+1} - f_{y_k} \sin\theta_{\ell,\ell+1} \\ f_{n_{k+1}} &= f_{z_{k+1}} \cos\theta_{\ell,\ell+1} - f_{y_{k+1}} \sin\theta_{\ell,\ell+1} \end{aligned} \tag{2.38}$$

$$\underset{\sim}{f}_k = \int_{V_k} \underset{\sim}{B}^{t}\ \underset{\sim}{\sigma}\ dV_k \tag{2.39}$$

If inequality Eq. (2.9d) is satisfied, $p_{\ell,k}$ becomes the master segment pressure, otherwise the contribution to the pressure of the next overlapping slave element is computed.

$$p_{\ell,k+1} = (S_{\ell,k+2} - S_{\ell,k+1})\ \sigma_{\ell}^{k+1} / S_{\ell} \tag{2.40}$$

If Eq. (2.11b) is not satisfied, k is incremented by 1 and the procedure given by Eqs. (2.11) and (2.40) continues until Eq. (2.11b) is satisfied. The total pressure for master segment ℓ is then given by Eq. (2.41); the summation is performed over all of the slave segments in contact with the master segment.

$$p_{\ell} = \sum_{i=0}^{n-1} p_{\ell,k+i} \tag{2.41}$$

The nodal forces acting at master node ℓ due to the pressure distribution on master segments ℓ-1 and ℓ are

$$\begin{aligned} f_{y_{\ell}} &= \tfrac{1}{2}\left[(z_{\ell}-z_{\ell-1})p_{\ell-1} + (z_{\ell+1}-z_{\ell})p_{\ell}\right] \\ f_{z_{\ell}} &= -\tfrac{1}{2}\left[(y_{\ell}-y_{\ell-1})p_{\ell-1} + (y_{\ell+1}-y_{\ell})p_{\ell}\right] \end{aligned} \tag{2.42}$$

2.4.7 Interface forces and master surface acceleration

The interface force calculation is based on the TENSOR algorithm. At master node ℓ, the normal interface force, $\Delta f_{n_{\ell}}$, is given by Eq. (2.43).

$$\Delta f_{n_{\ell}} = \frac{\Delta M_{\ell} F_{n_{\ell}} - M_{\ell} f_{n_{\ell}} + M_{\ell} M_{\ell} a_c}{M_{\ell}^{+}} \tag{2.43}$$

where

$$F_{n_{\ell}} = M_{\ell}(\ddot{z}_{\ell} \cos\theta_{\ell-1,\ell+1} - \ddot{y}_{\ell}\sin\theta_{\ell-1,\ell+1})$$

$$f_{n_{\ell}} = f_{z_{\ell}} \cos\theta_{\ell-1,\ell+1} - f_{y_{\ell}} \sin\theta_{\ell-1,\ell+1}$$

and a_c is the Coriolis acceleration defined in Eq. (2.15).

Normal and tangential accelerations of the ℓth master node are:

$$\ddot{a}_{n_\ell} = (F_{n_\ell} - \Delta f_{n_\ell}) / M_\ell$$
$$\ddot{a}_{t_\ell} = \ddot{y}_\ell \cos\theta_{\ell-1,\ell+1} + \ddot{z}_\ell \sin\theta_{\ell-1,\ell+1} \qquad (2.44)$$

The global accelerations can now be found from Eq. (2.6).

2.4.8 Slave node accelerations and velocities

The preceding steps have determined the motion of the master surface and have left unchanged the motion of the slave surface. As might be expected, the motion of slave nodes not in contact with the master surface is unaffected, but the motion of those slave nodes in contact with the master surface must be adjusted to ensure that the latter nodes remain so. In the procedure used here, the velocities and accelerations normal to the master line are reset. Although no guarantee exists in the present algorithm that slave nodes will remain exactly on the master surface, in practice, excursions away from the master surface have proven to be negligible.

Considering each slave node in turn, the first step is to compute the tangential velocity and acceleration. For the kth slave node on the ℓth master segment, these quantities are given by Eq. (2.45), where ψ_k measures the angle of the slideline at the location of node k.

$$v_{k_t} = \dot{\bar{y}}_k \cos\psi_k + \dot{\bar{z}}_k \sin\psi_k$$
$$a_{k_t} = \ddot{\bar{y}}_k \cos\psi_k + \ddot{\bar{z}}_k \sin\psi_k \tag{2.45}$$

We shall discuss the choice of ψ_k later. The normal components of velocity and acceleration are interpolated from the master nodes. For example Eq. (2.46) defines the normal component of the velocity for node k sliding on master segment ℓ.

$$v_{k_n} = (1-\alpha_k)\,[\dot{z}_\ell \cos\psi_k - \dot{y}_\ell \sin\psi_k] + \alpha_k\,[\dot{z}_{\ell+1} \cos\psi_k - \dot{y}_{\ell+1} \sin\psi_k] \tag{2.46}$$

A normal acceleration component, a_{k_n}, is likewise defined. After the tangential and normal components of the acceleration and velocity are known, the new accelerations are given by Eq. (2.47), where the last term is the Coriolis term and $\dot{y}_{k_r}$, $\dot{z}_{k_r}$ define the relative velocities between master segment ℓ and node k.

$$\ddot{\bar{y}}_k^{n+1} = a_{k_t} \cos\psi_k - a_{k_n} \sin\psi_k - 2\omega\dot{z}_{k_r}$$
$$\ddot{\bar{z}}_k^{n+1} = a_{k_t} \sin\psi_k + a_{k_n} \cos\psi_k + 2\omega\dot{y}_{k_r} \tag{2.47}$$

$$\omega = (v_{n_{\ell+1}} - v_{n_\ell}) / S_\ell \tag{2.48}$$

$$\dot{y}_{k_r} = \dot{y}_k - (1-\alpha_k)\dot{y}_\ell - \alpha_k \dot{y}_{\ell-1}$$
$$\dot{z}_{k_r} = \dot{z}_k - (1-\alpha_k)\,\dot{z}_\ell - \alpha_k\,\dot{z}_{\ell+1} \tag{2.49}$$

The new velocities are the by now familiar combination of the tangential components from the slave side and normal components from the master side.

$$y_k = v_{k_t} \cos\gamma_k - v_{k_n} \sin\gamma_k$$
$$z_k = v_{k_t} \sin\gamma_k + v_{k_n} \cos\gamma_k \qquad (2.50)$$

Throughout the development of our slideline logic we have studied the choice of ψ_k on the results of a large number of applications. In our first implementation of the slideline logic we set

$$\begin{aligned} \psi_k &= \theta_{\ell,\ell+1} && \varepsilon \le \alpha_k \le 1-\varepsilon \\ \psi_k &= \theta_{\ell-1,\ell+1} && \alpha_k < \varepsilon \\ \psi_k &= \theta_{\ell,\ell+2} && \alpha_k > 1-\varepsilon \end{aligned} \qquad (2.51)$$

where ε is typically set to 10^{-3}. We found that this choice created numerical noise in some calculations, usually in the form of hourglassing, and that computing ψ_k as the normal to a quadratic curve through the closest master node and two adjacent nodes eliminated much of the noise. If ℓ is the closest master node then Eq. (2.52) is the parametric equation for a parabola where the parametric coordinate ξ is bounded in the interval from -1 to 1 inclusive. Angle ψ_k is now based on the slope of Eq. (2.52).

$$y(\xi) = \tfrac{1}{2}\,\xi(\xi-1)y_{\ell-1} + (1-\xi^2)y_\ell + \tfrac{1}{2}\,\xi(\xi+1)y_{\ell+1}$$
$$z(\xi) = \tfrac{1}{2}\,\xi(\xi-1)z_{\ell-1} + (1-\xi^2)z_\ell + \tfrac{1}{2}\,\xi(\xi+1)z_{\ell+1} \qquad (2.52)$$

$$\psi_k = \cos^{-1} \{ \frac{dy}{d\xi} / [(\frac{dy}{d\xi})^2 + (\frac{dz}{d\xi})^2]^{1/2} \}_{\xi=\alpha_k} \qquad (2.53)$$

We assume that node k is sliding on master segment ℓ. If $\ell+1$ is the closest node to k, the foregoing procedure Eqs. (2.52)-(2.53) is repeated with ℓ increased by 1 and ξ is α_k-1. Eqs. (2.52) and (2.53) are used in the public domain versions of DYNA2D.

Using Eq. (2.53) to determine ψ_k leads to the same kind of noise as Eq. (2.51) though not as pronounced. We can illustrate this noise with the concentric spheres in Fig. 8 which have the bulk modulus of steel and no shear strength. The spheres are 1 centimeter thick and 7.5 and 8.5 centimeters in radius. A 100 kilabar pressure is applied to the outer surface to push the spheres inward. The result is shown in Fig. 9, where the slave surface, chosen to be the inner surface, has elements that have hourglassed and sheared. This anomalous behavior is related to our choice for ψ_k. If we choose the normal to the slave surface at k, Eq. (2.54), we get the more pleasing result in Fig. 10.

$$\psi_k = \theta_{k-1,k+1} \qquad (2.54)$$

We can expect separation between the master and slave surfaces if normals are based on Eq. (2.54). In many of our calculations we have found the separation or inner penetration to be very small, but in other calculations the separation or overlap is noticeable. In these latter cases very slight adjustments to the normal slave velocity is all that is necessary to keep the slave nodes close to the surface. We now use the normal distance from the slave node to the master surface to compute the velocity change required to close the gap, and we adjust the normal

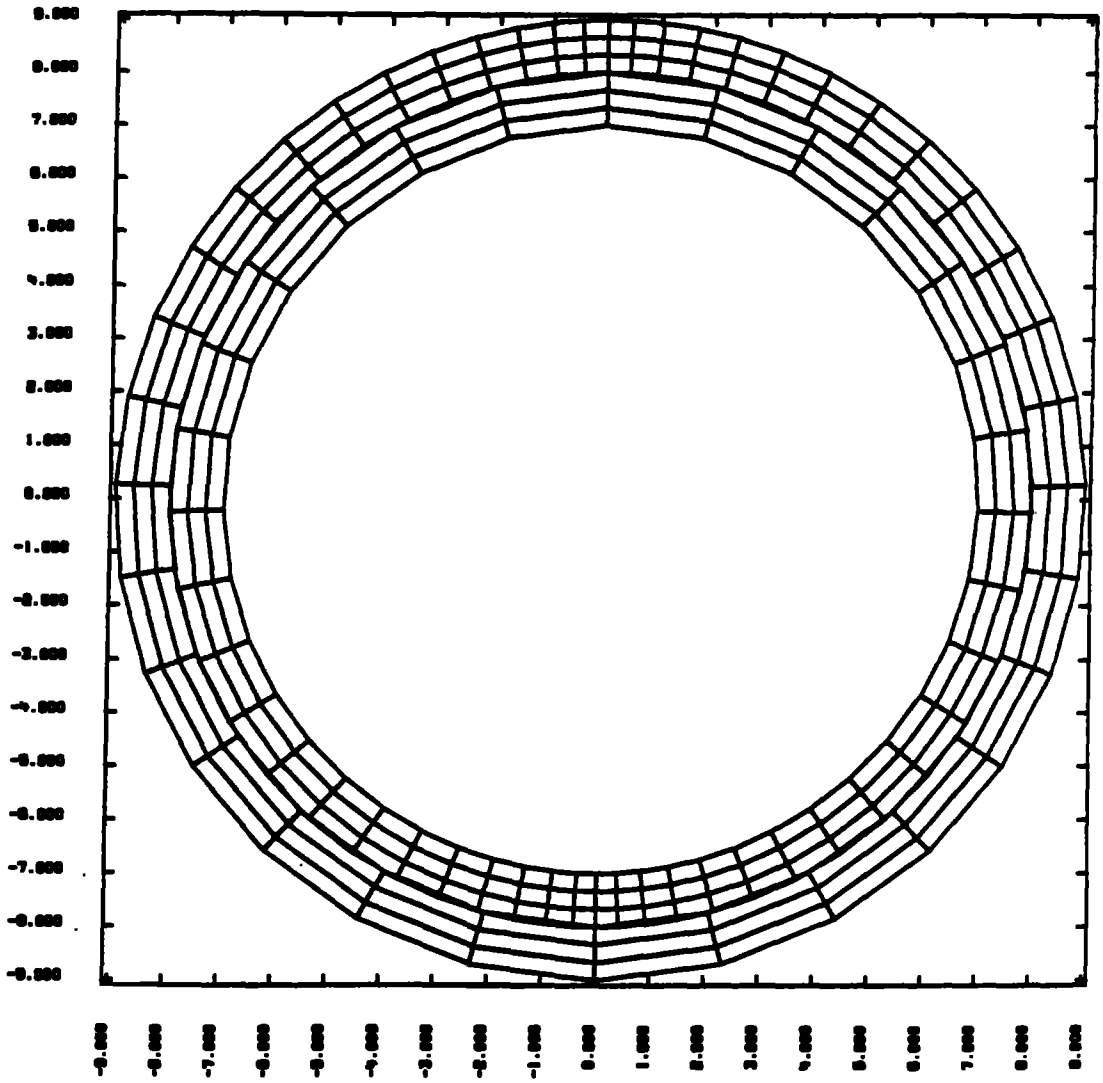

Fig. 8. Initial geometry of concentric spheres. A 100 kbar pressure is applied to the outer surface to push the spheres inward.

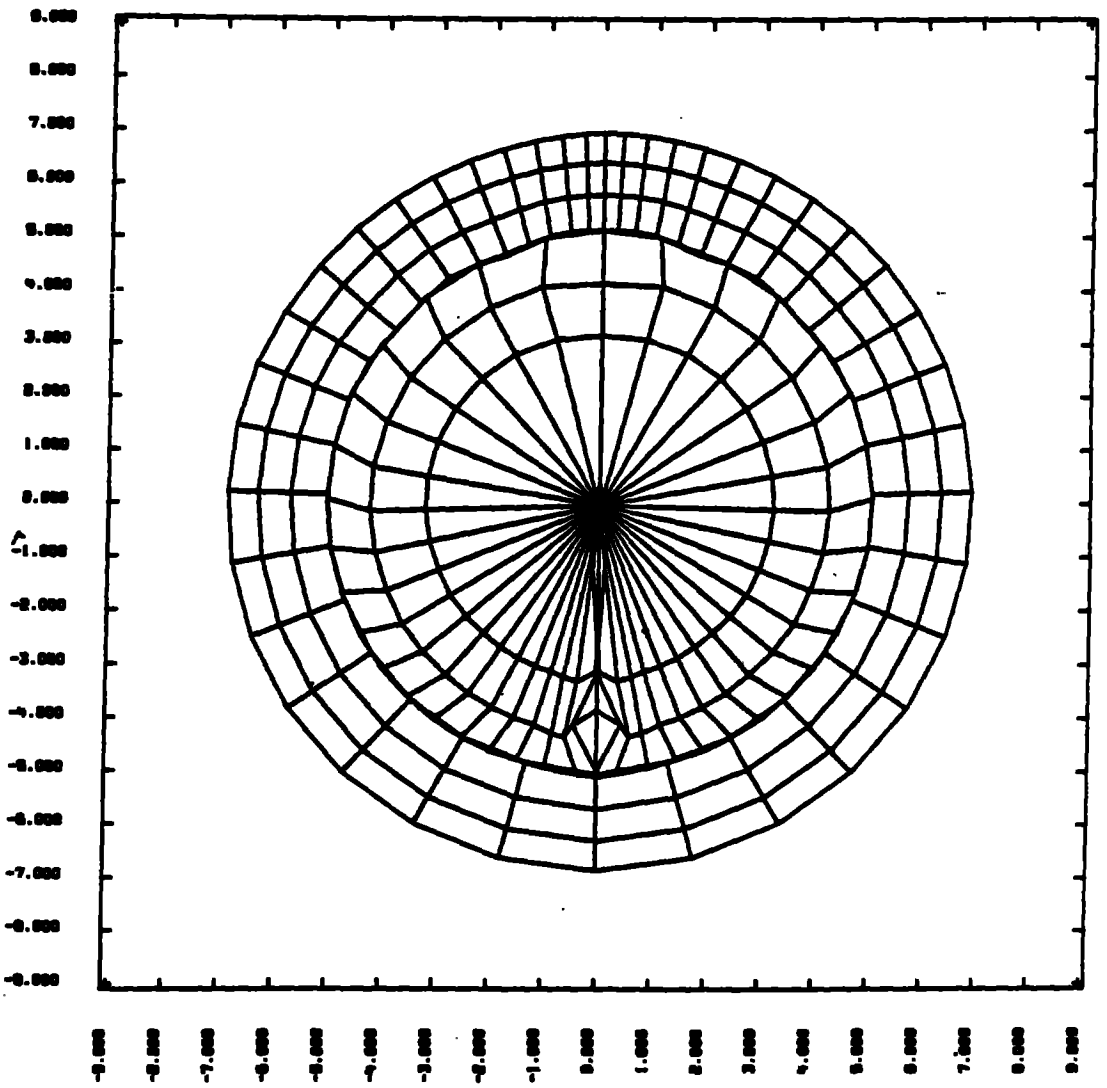

Fig. 9. Improper interface normal leads to anomalous behavior.

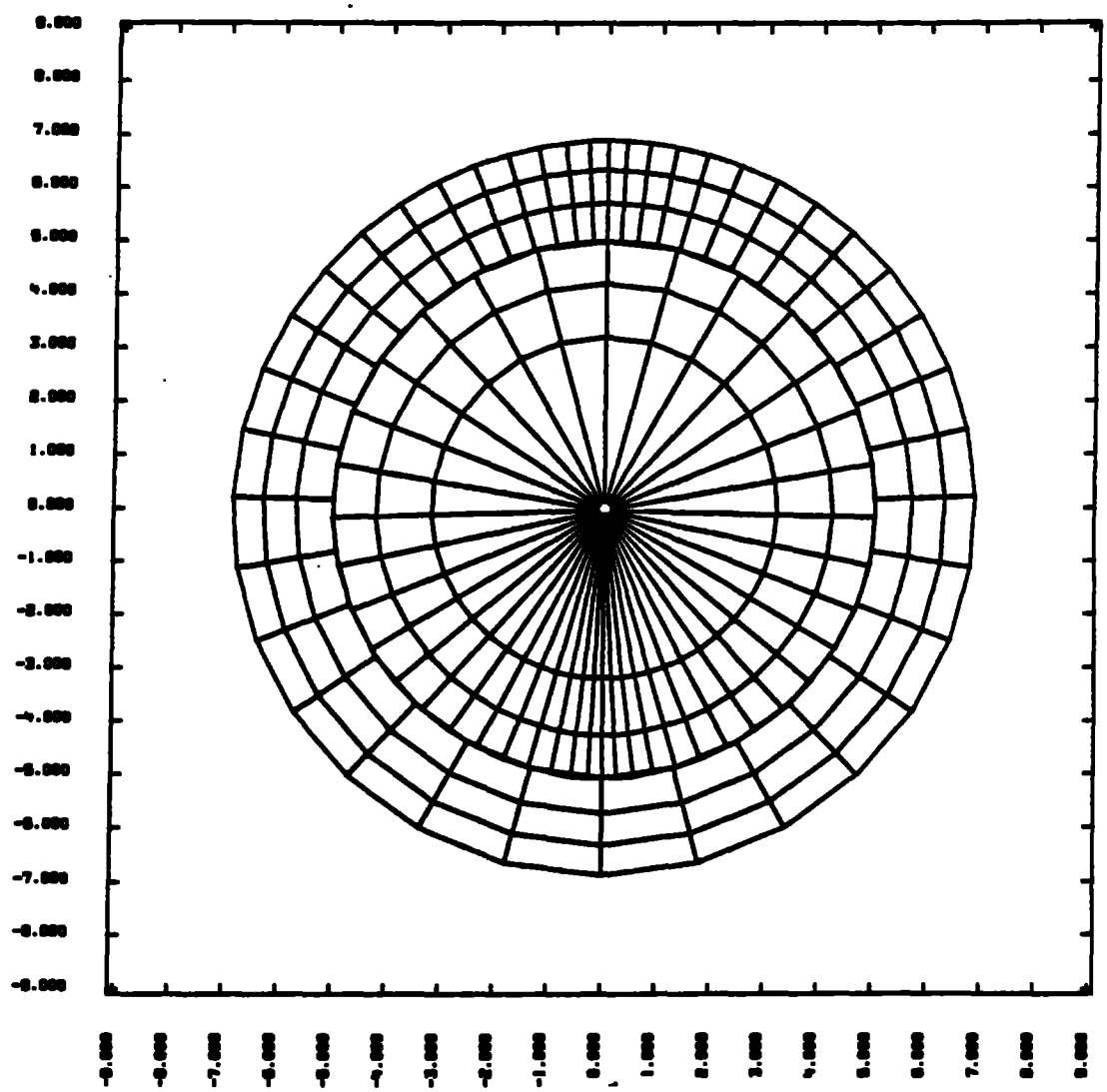

Fig. 10. Proper interface normal leads to the correct result.

slave velocity each time step by 1 percent of this change. Thus, the slave node is never returned to the master surface; it is just kept reasonably close. We have not found momentum conservation to be significantly affected and, in fact, it has sometimes been better than with our old approach.

2.4.9 Time step calculation

Before updating the configuration to t^{n+1}, every slave node that is not in contact with the master line is checked to determine if it will penetrate the master line between time t^n and t^{n+1}. If any slave node penetrates, $\Delta t^{n+1/2}$ is scaled back such that no slave node penetrates but at least one slave node reaches the master surface. At the beginning of the next time step impact conditions are applied to the slave nodes that reached the master line and constraints are imposed to keep the nodes in contact with the master line.

Consider slave node k that is close to but not in contact with the master line at time t^n. The first step in determining penetration is to locally update the geometry of node k and nearby master nodes. After the closest master node is located, the master segment associated with slave node k is found using Eqs. (2.18) and (2.19). Let master segment ℓ be associated with slave node k. If Eq. (2.55) is satisfied, where $\underset{\sim}{m}_\ell$ is the outward drawn unit vector normal to master segment ℓ, penetration has occurred.

$$\underset{\sim}{r}_{\ell k} \cdot \underset{\sim}{m}_\ell < 0 \qquad (2.55)$$

If slave node k penetrates master segment ℓ, the maximum permissible time step size is computed that will not allow node k to

penetrate. This time step size is found by equating the slope of master segment ℓ with the line drawn from node ℓ to k at $t^n + \Delta t$. If the velocities are assumed to be constant, a quadratic equation is obtained for Δt.

2.4.10 Simplifications

We have attempted to increase the efficiency of the foregoing algorithm by making two reasonable approximations. In the first we replace the calculation for m_k in Eq. (2.25) with an approximation using the mass matrix.

$$m_k = \frac{1}{2} L_k \, (m_k^* + m_{k+1}^*) \tag{2.56}$$

$$m_k^* = 2M_k \; / \; |\underset{\sim}{r}_{k-1,k+1}|$$

M_k is the global mass at slave node k, and $|\underset{\sim}{r}_{k-1,k+1}|$ denotes the length of the vector from k-1 to k+1. In the second approximation we replace calculations to obtain σ_ℓ^k in Eq. (2.37) by

$$\sigma_\ell^k = \frac{1}{2} \, (\sigma_k^* + \sigma_{k+1}^*) \tag{2.57}$$

$$\sigma_k^* = 2 \cdot (F_{z_k} \cos\theta_{k-1,k+1} - F_{y_k} \sin\theta_{k-1,k+1}) \; / \; |\underset{\sim}{r}_{k-1,k+1}|$$

F_{y_k} and F_{z_k} are the global forces at slave node k before accounting for the slideline coupling.

We have vectorized the slideline logic that includes these simplifications and, consequently, have reduced the cost significantly for what seems to be only a minor difference in the results due to the averaging.

2.4.11 Extension of hydrocode algorithm to 3D

We have implemented the sliding interface algorithm without separation between the surfaces into DYNA3D. Because we know of no reasonable way to economically map the slave surface on to the master surface for the distribution of mass and pressure, the simplifications of Section 2.4.10 are used in the 3D extension.

3. PENALTY FORMULATION

The computer implementation of the penalty formulation in explicit codes is straightforward. The interface subroutines are called each time step prior to computing the accelerations. In the implicit codes the interfaces are treated like another element class. We reform the stiffness matrix at the beginning of each time step taking into account the changing connectivity along the interfaces; consequently, we do not limit the relative displacement. We also reform during the equilibrium iterations if convergence problems arise. Bandwidth minimization is performed at the beginning of the problem and is based on the initial coupling across the interface.

In two dimensions, the slideline definitions are identical to the DYNA2D hydrocode algorithm. In three dimensions, all triangular and quadrilateral segments in each surface are required as input with an arbitrary ordering of the segments. In the development that follows, we refer to one surface as the slave and the other as the master even though the symmetry of our approach eliminates any bias in this choice.

Initialization of the penalty method in two dimensions involves several steps. First, we reverse the ordering of the nodes along the slave side so that as one moves along the slave surface in the order

that the slave nodes appear, the master surface will be to the left, and then we check each master and slave node for penetration through the slave and master surfaces, respectively. Penetrating nodes are projected back on to the surface. Finally, for each master and slave segment, we find the element that contains the segment in its connectivity and compute a segment stiffness as a function of the bulk modulus and thickness. The second step eliminates the possibility of large forces developing due to interpenetration of nodes along a curved interface due to discretization differences across the interface, and the third step ensures a reasonable value for the interface stiffness.

In the three dimensional initialization we first gather all the slave and master nodes into arrays and store the segment numbers that contain each node. The second and third steps are the same.

A general interface treatment using penalty functions may be outlined as follows:

1. For each slave node, n_s, locate the closest master node, n_m, and check the master segments that include n_m to identify the segment, if any, containing n_s.
2. Locate the position of the slave node on the master surface.
3. Determine if n_s has penetrated the master segment. If so, compute and add an interface force to the right hand side and, if the global stiffness matrix is being reformed, add in an interface stiffness matrix.
4. Repeat steps 1-3 for the master nodes.

3.1 Determination of Master Segment Containing Slave Node

Consider a slave node, n_s, sliding on a piecewise smooth master surface and assume that search of the master surface has located and

stored the master node, n_m, lying closest to n_s. Fig. 11 depicts a portion of a master surface with nodes n_m and n_s labeled. To minimize the operation count, the search for the closest node only includes the closest node from the previous time step, n_m^{old} and its surrounding nodes which are available in the connectivities of the segments that contain n_m^{old}.

If m_s and n_s do not coincide, n_s can usually be shown to lie in a segment s_i via the following tests:

$$(\underset{\sim}{c}_i \times \underset{\sim}{s}) \cdot (\underset{\sim}{c}_i \times \underset{\sim}{c}_{i+1}) > 0$$
$$(\underset{\sim}{c}_i \times \underset{\sim}{s}) \cdot (\underset{\sim}{s} \times \underset{\sim}{c}_{i+1}) > 0 \qquad (3.1)$$

Vectors $\underset{\sim}{c}_i$ and $\underset{\sim}{c}_{i+1}$ are along edges of s_i and point outward from m_s, and vector $\underset{\sim}{s}$ is the projection of the vector beginning at m_s, ending at n_s, and denoted by $\underset{\sim}{g}$, on to the plane being examined (see Fig. 12).

$$\underset{\sim}{s} = \underset{\sim}{g} - (\underset{\sim}{g} \cdot \underset{\sim}{m})\ \underset{\sim}{m}$$
$$\underset{\sim}{m} = \frac{\underset{\sim}{c}_i \times \underset{\sim}{c}_{i+1}}{|\underset{\sim}{c}_i \times \underset{\sim}{c}_{i+1}|} \qquad (3.2)$$

Since the sliding constraints keep n_s close but not necessarily on the master surface and since n_s may lie near or even on the intersection of two master segments, the inequalities of Eqs. (3.1) may be inconclusive, i.e., they may fail to be satisfied or more than one may give positive results. When this occurs n_s is assumed to lie along the intersection which yields the maximum value for the quantity defined in Eq. (3.3).

$$\frac{\underset{\sim}{g} \cdot \underset{\sim}{c}_i}{|\underset{\sim}{c}_i|} \qquad i = 1,2,3,4... \qquad (3.3)$$

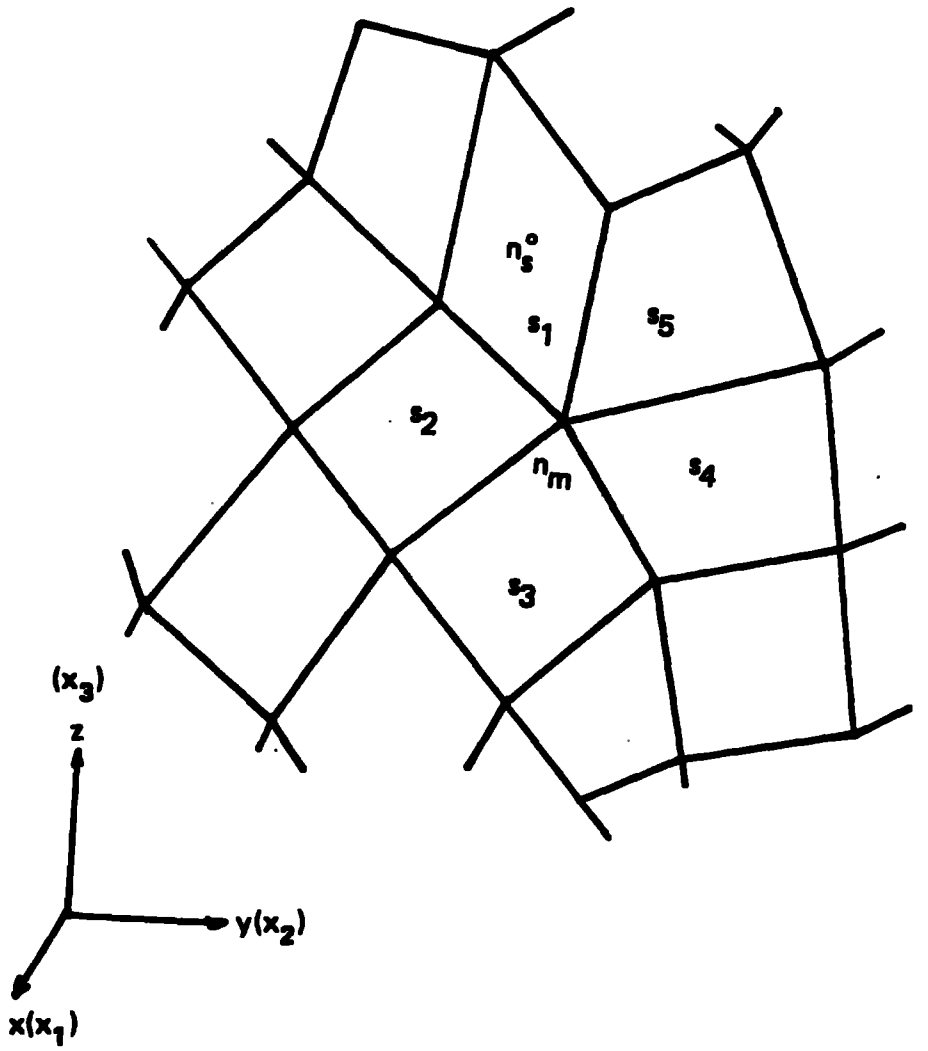

Fig. 11. In this figure, five master segments can harbor slave node n_s given that n_m is the closest master node.

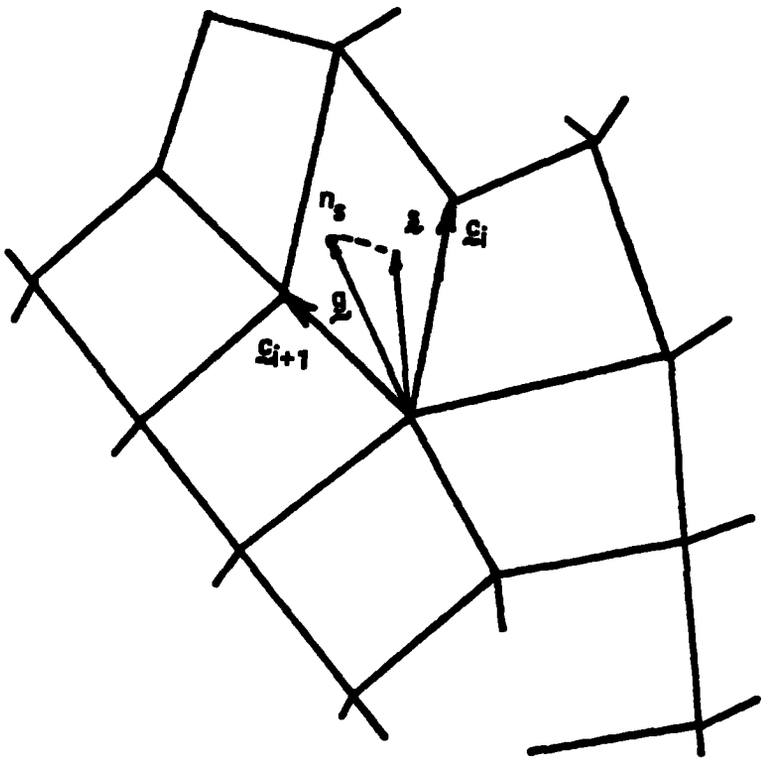

Fig. 12. Projection of g into master segment s_1.

The test Eq. (3.1) is first applied to the master segment that contained the slave node in the previous step. If Eq. (3.1) is not satisfied, then each master segment that includes n_m is checked. Our implementation does not limit the number of segments that may contain n_m.

3.2 Determination of the Contact Point

Assume that a master segment has been located for slave node, n_s, and that n_s is not identified as lying on the intersection of two master segments. Then we may identify the "contact point", defined as the point on master segment which is closest to n_s. Each master surface segment, s_i has a bilinear parametric representation.

$$\underset{\sim}{r} = f_1(\xi,\eta)\underset{\sim}{i}_1 + f_2(\xi,\eta)\underset{\sim}{i}_2 + f_3(\xi,\eta)\underset{\sim}{i}_3 \tag{3.4}$$

$$f_i(\xi,\eta) = \sum_{j=1}^{4} \phi_j \, x_i^j \tag{3.5}$$

$$\phi_j(\xi,\eta) = \frac{1}{4}(1 + \xi\xi_j)(1 + \eta\eta_j)$$

ξ_j, η_j take on their nodal values at $(\pm 1, \pm 1)$, and x_i^j is the nodal coordinate of the jth node in the ith direction, see Fig. 13. Note that $\underset{\sim}{r}$ is at least once continuously differentiable and that the normal is nonzero.

$$\frac{\partial \underset{\sim}{r}}{\partial \xi} \times \frac{\partial \underset{\sim}{r}}{\partial \eta} \neq 0 \tag{3.6}$$

Thus, $\underset{\sim}{r}$ represents a master segment that has a unique normal whose direction depends continuously on the points of s_i.

Let $\underset{\sim}{t}$ be a position vector drawn to slave node n_s and assume that the master surface segment s_1 has been identified with n_s. The contact point coordinates (ξ_c, η_c) on s_1 must satisfy Eq. (3.7).

$$\frac{\partial \underset{\sim}{r}}{\partial \xi}(\xi_c, \eta_c) \cdot [\underset{\sim}{t} - \underset{\sim}{r}(\xi_c, \eta_c)] = 0 \qquad (3.7a)$$

$$\frac{\partial \underset{\sim}{r}}{\partial \eta}(\xi_c, \eta_c) \cdot [\underset{\sim}{t} - \underset{\sim}{r}(\xi_c, \eta_c)] = 0 \qquad (3.7b)$$

The physical problem is illustrated in Fig. 13 which shows n_s lying above the master surface. Eqs. (3.7a) and (3.7b) are readily solved for ξ_c in terms of η_c. One way to accomplish this is to solve Eq. (3.7a) for ξ_c in terms of η_c, and substitute the result into Eq. (3.7b). This yields an equation in η_c which is presently solved numerically in DYNA3D.

3.3 Nodal Force Update

Each slave node is checked for penetration through its master segment. If the slave node does not penetrate, nothing is done, but if it does, an interface force is applied between the slave node and its contact point. The magnitude of this force is proportional to the amount of penetration.

Penetration of the slave node n_s, through the master segment s_1, which contains its contact point is indicated if ℓ is negative.

$$\ell = \underset{\sim}{n}_1 \cdot [\underset{\sim}{t} - \underset{\sim}{r}(\xi_c, \eta)] < 0 \qquad (3.8)$$

$$\underset{\sim}{n}_1 = \underset{\sim}{n}_1(\xi_c, \eta_c) = \left(\frac{\partial \underset{\sim}{r}}{\partial \xi} \times \frac{\partial \underset{\sim}{r}}{\partial \eta}\right) \Big/ \left|\frac{\partial \underset{\sim}{r}}{\partial \xi} \times \frac{\partial \underset{\sim}{r}}{\partial \eta}\right|$$

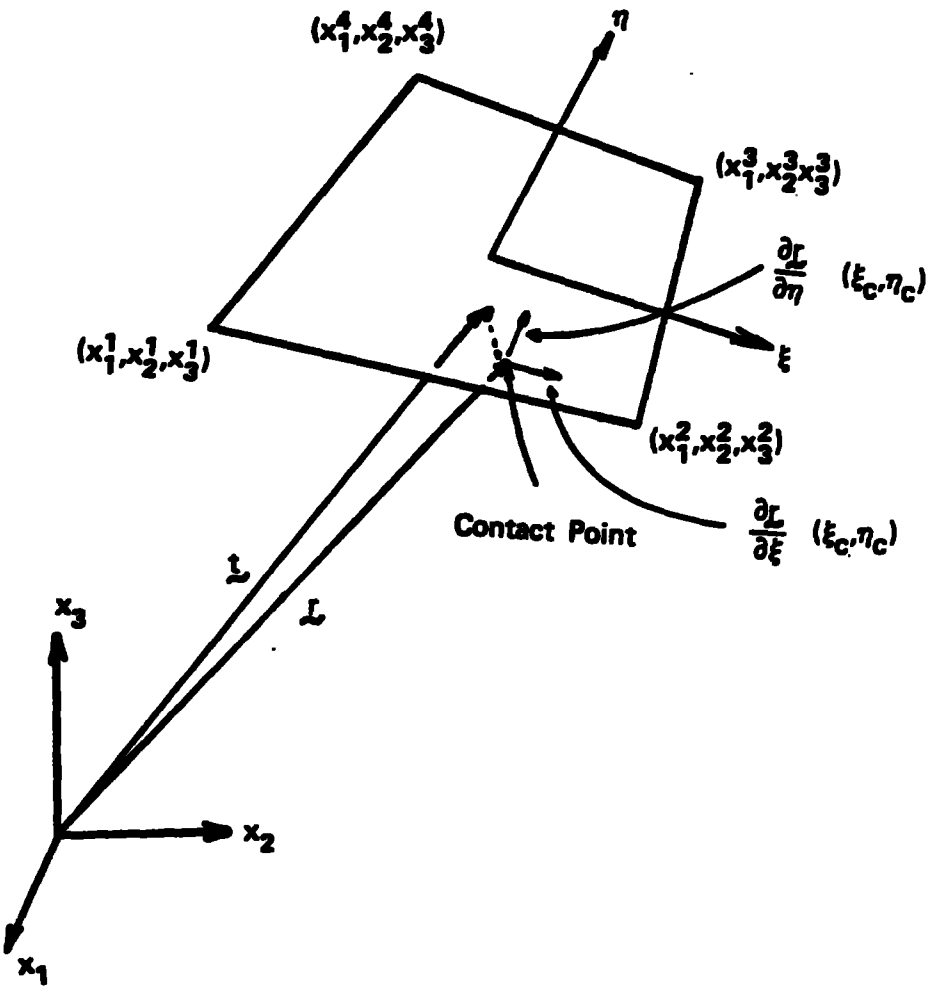

Fig. 13. Location of contact point when n_s lies above master segment. is normal to the master segment at the contact point.

If slave node n_s has penetrated through master segment s_1, we add an interface force vector $\underset{\sim}{f}_s$ that is normal to the master segment and linearly dependent on the penetration to node n_s.

$$\underset{\sim}{f}_s = - \ell k_i \underset{\sim}{n}_i \qquad \text{if } \ell < 0 \tag{3.9}$$

An equal and opposite force is distributed over the master segment nodes according to Eq. (3.10).

$$\underset{\sim}{f}^i_m = - \phi_i(\xi_c, \eta_c)\underset{\sim}{f}_s \qquad \text{if } \ell < 0 \tag{3.10}$$

The stiffness factor k_i for master segment s_i is given in terms of the bulk modulus, K_i, the volume V_i, and the face area, A_i, of the element that contains s_i as

$$k_i = \frac{f_{SI} K_i A_i^2}{V_i} \tag{3.11}$$

where f_{SI} is a scale factor for the interface stiffness and is normally defaulted to .10. Larger values may cause instabilities unless the time step size is scaled back in the time step calculation.

4. EXAMPLES

We present in this section five examples from diverse applications where contact-impact algorithms are necessary. None of these examples were run just for this paper; they were run on the production versions of our codes in the production-oriented engineering environment at LLNL.

1. Mass Focused Projectiles

Our first example demonstrates the hydrodynamic approach to contact implemented in DYNA3D.

Mass focused projectiles, also called Misznay-Schardin munitions, are being designed as anti-armor devices. This kind of munition uses high explosives to accelerate a metal plate to a high velocity. As the

plate accelerates, it is designed to deform into a cohesive shape that can penetrate thick armor. Furthermore, its shape must provide aerodynamic stability to accommodate long standoffs from the target. Computer codes are used to iteratively develop a design with all the desired properties. Testing of the design follows to insure that everything performs as predicted.

Tuft and Godfrey [16], have computed fully three-dimensional geometries such as shown in Figs. 14 and 15 with two planes of symmetry. The time sequence of two liner cross sections is shown in Fig. 16.

Slidelines are used between the high explosive and the liner and the case to allow the gas from the explosion to expand without restriction. The deformed shape of the liner is very sensitive to the pressure history, therefore both the detonation wave front and explosive-liner interface must be modeled carefully.

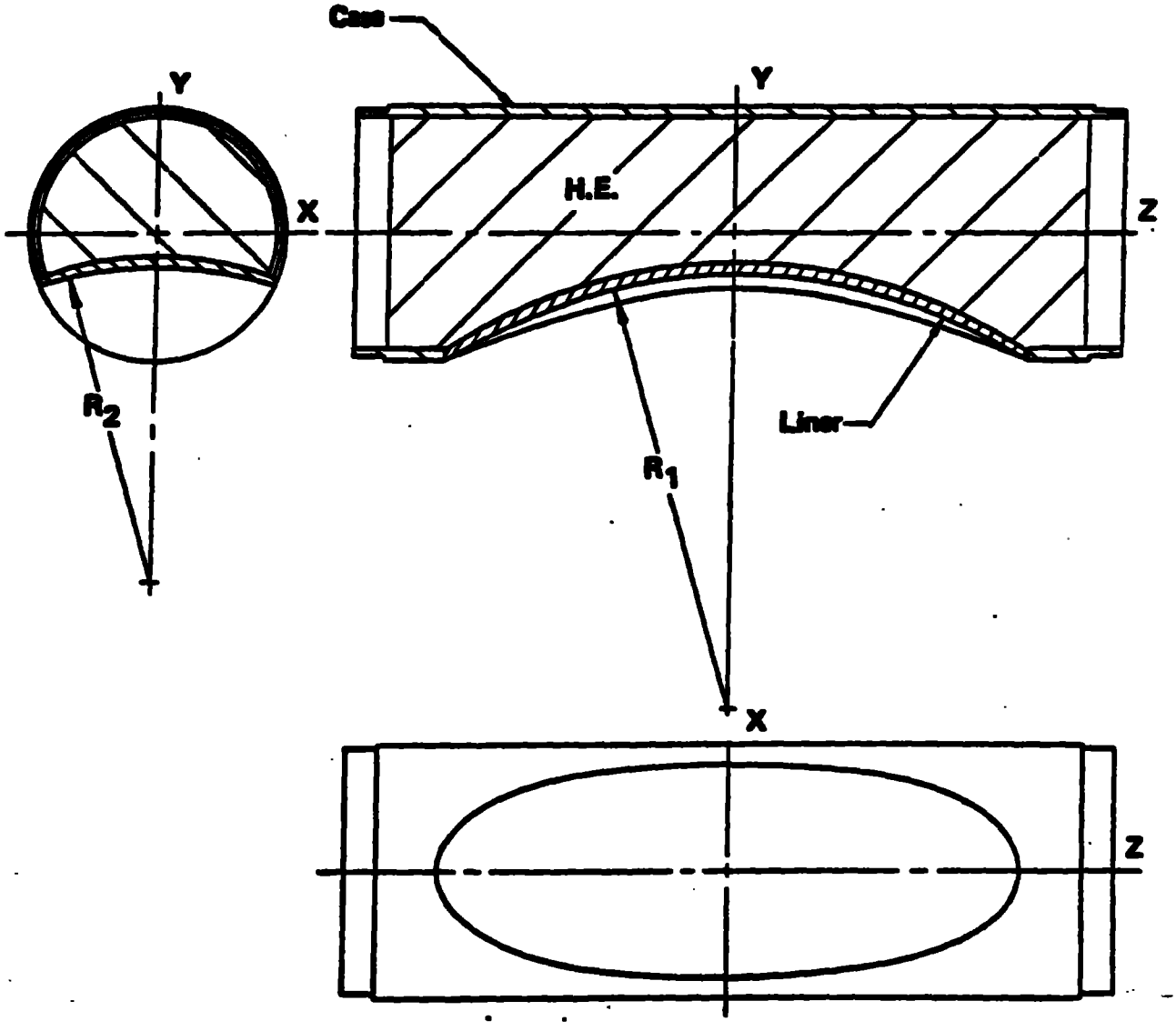

Fig. 14. Basic geometry for 3D mass focused projectile device.

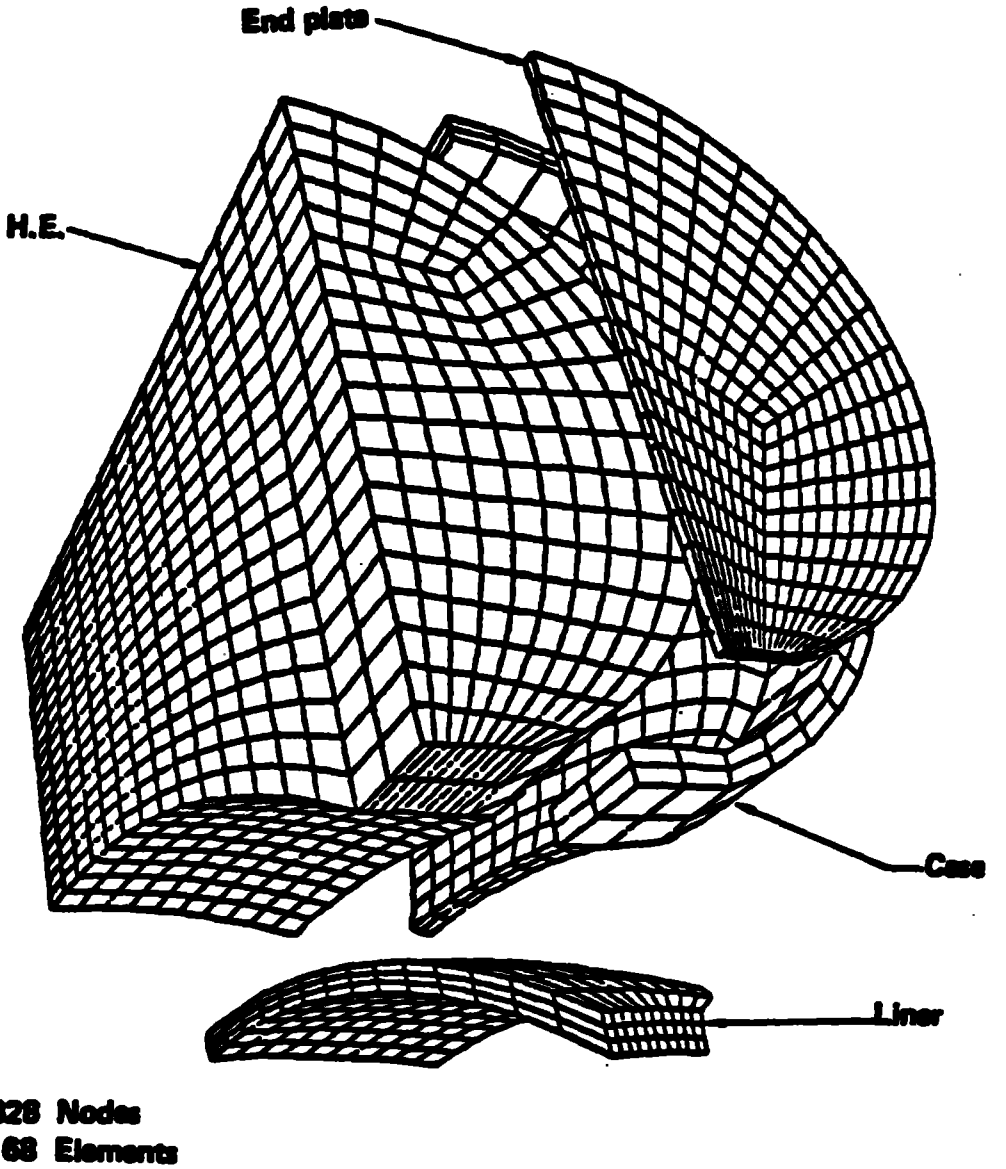

Fig. 15. Three-dimensional finite-element mesh.

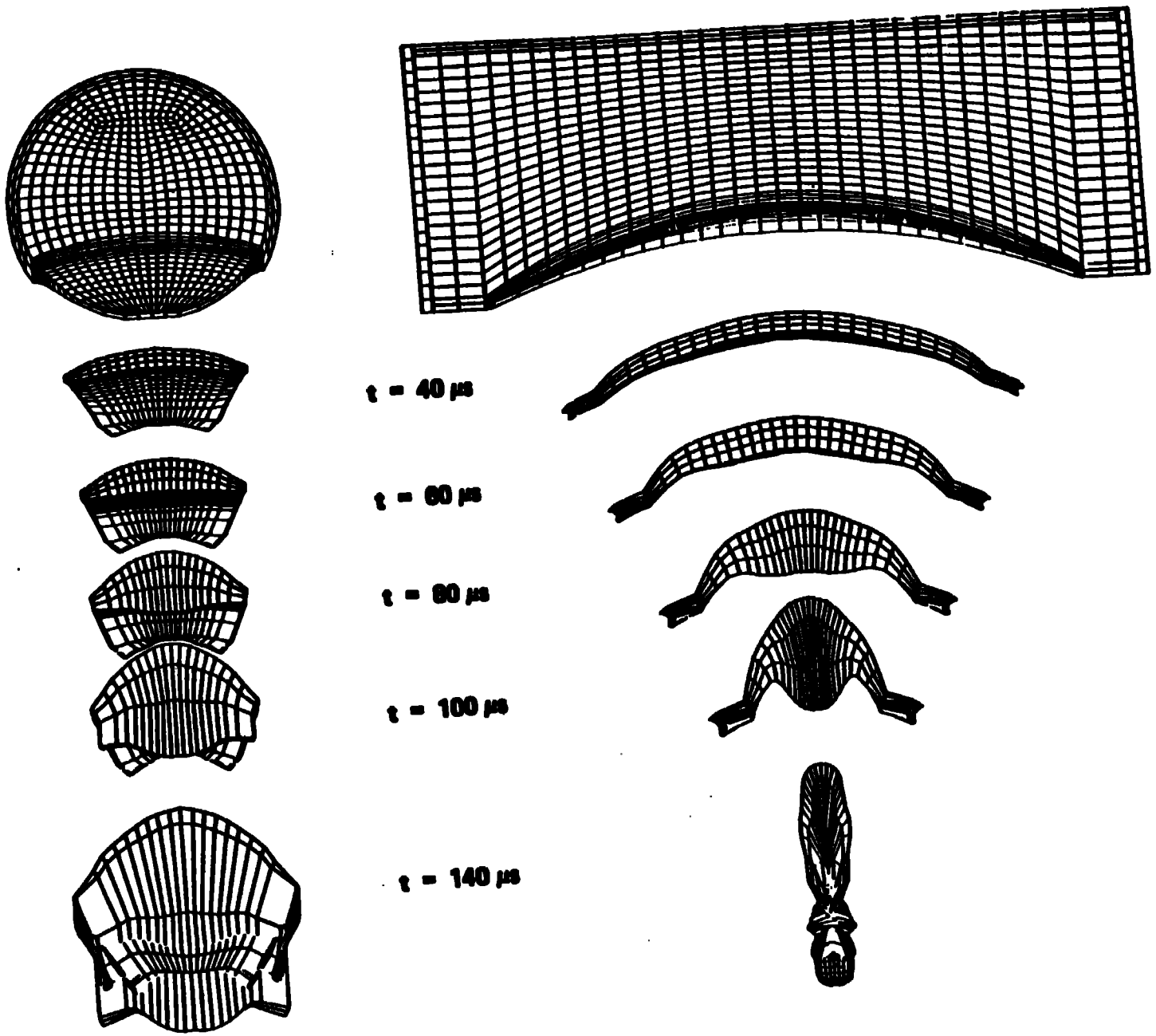

Fig. 16. Time sequence of two liner cross sections.

2. Bellows Forming Analysis

This example illustrates a problem involving a large amount of sliding along the contact interface. The purpose of the calculation is to determine the pressure required to collapse the stainless steel sleeve into the elastic die. Fig. 17 depicts the calculational mesh and boundary conditions.

A pressure loading is applied in 43 equal increments to a peak value of .580 GPa and is removed in two increments for a total of 45 steps. When the pressure reaches .483 GPa, the sleeve is completely collapsed. A sequence of deformed shapes is shown in Fig. 18 followed by the final configuration in Fig. 19.

The analysis was performed using NIKE2D; the slideline uses the the penalty formulation.

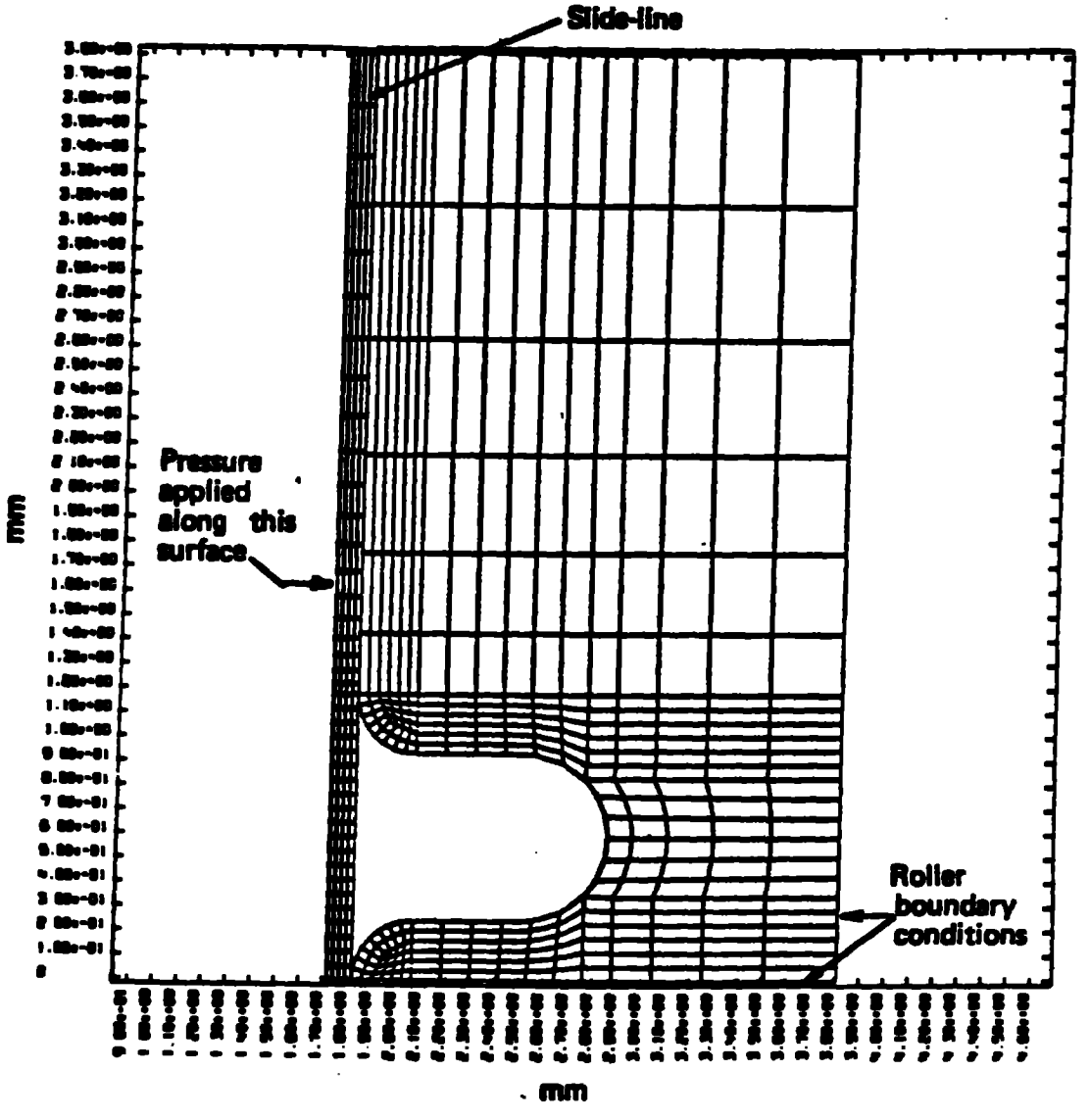

Fig. 17. Initial configuration.

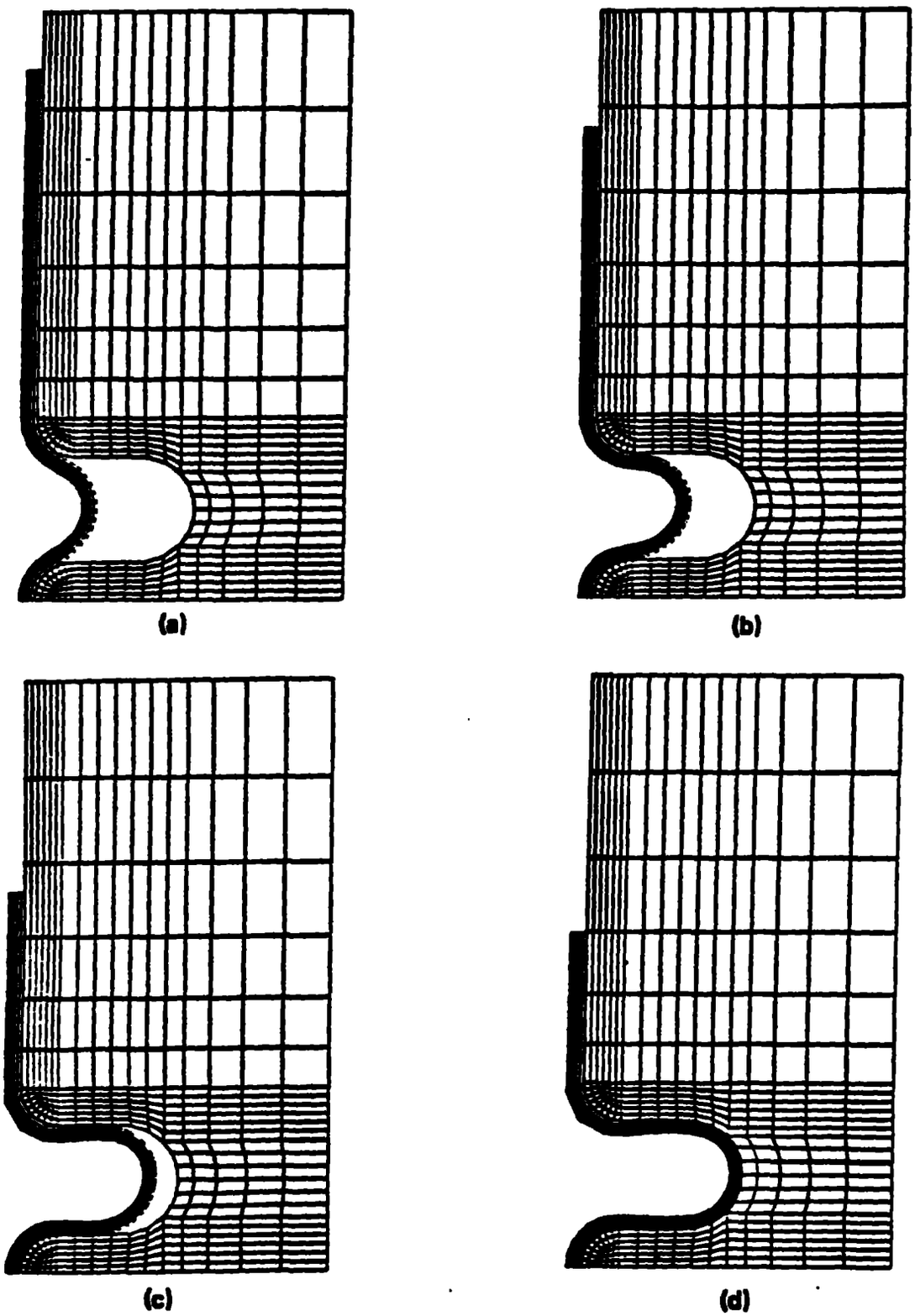

Fig. 18. Deformed shapes corresponding to pressures of (a) .138 GPa, (b) .276 GPa, and (d) .552 GPa.

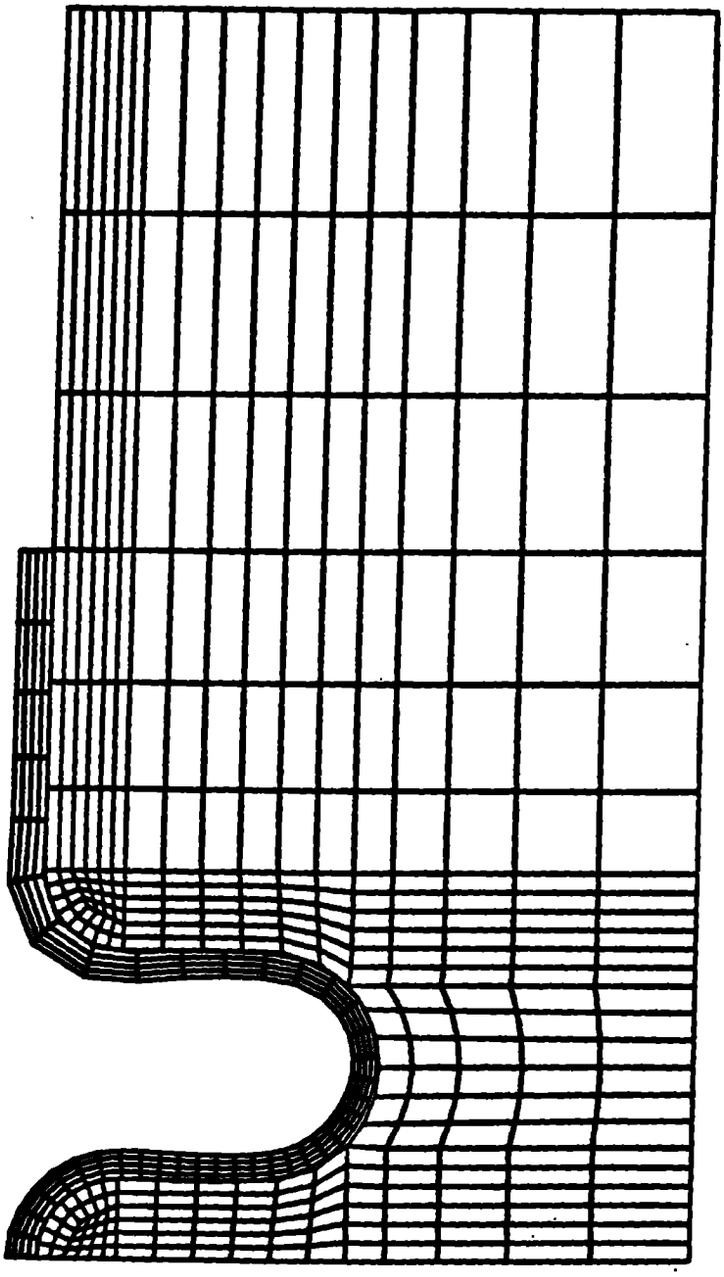

Fig. 19. Final deformed shape after removal of pressure.

3. METALLIC O-RING

In a recent application, standard metallic O-rings were failing to produce a reliable seal. The designers felt that these failures were due to large cutouts in one of the flanges. It was felt that these cutouts, which are required for the installation gas transfer fittings, reduced the rigidity of the flange to the point where the interface pressures were insufficient for sealing.

The following figures show the three-dimensional model which was used to analyze the problem. The mesh in Figs. 20 and 21 consists of 4816 nodal points and 3304 elements. Slidelines are defined between the upper portions of the O-ring and the upper flange, the lower portion of the O-ring and the lower flange, and the outer portion of the O-ring and the corresponding sealing surface of the lower flange. Additionally, a slide-surface is located between the two flanges. The model extends from the center of one of the cutouts to the center of a corresponding bolt hole. Symmetry planes are used at each of these locations to provide boundary conditions.

The total loading of the model occurs over fifteen steps. The first four steps crush the O-ring. During this portion of the loading, the O-ring undergoes large plastic strain and the interface pressures begin to develop. The next two steps are used to finish closing the gap between the two flanges. Steps eight through ten finish the bolt loading of the flanges. The upper bolt loads are sufficient to cause some plastic deformation of the upper flange. The last five steps are used to apply the gas pressure to the inside of the model. This pressurization partially unloads the O-ring. Fig. 22 shows a result of the calculation.

The NIKE3D analysis clearly showed that the cutouts were not causing the failures.

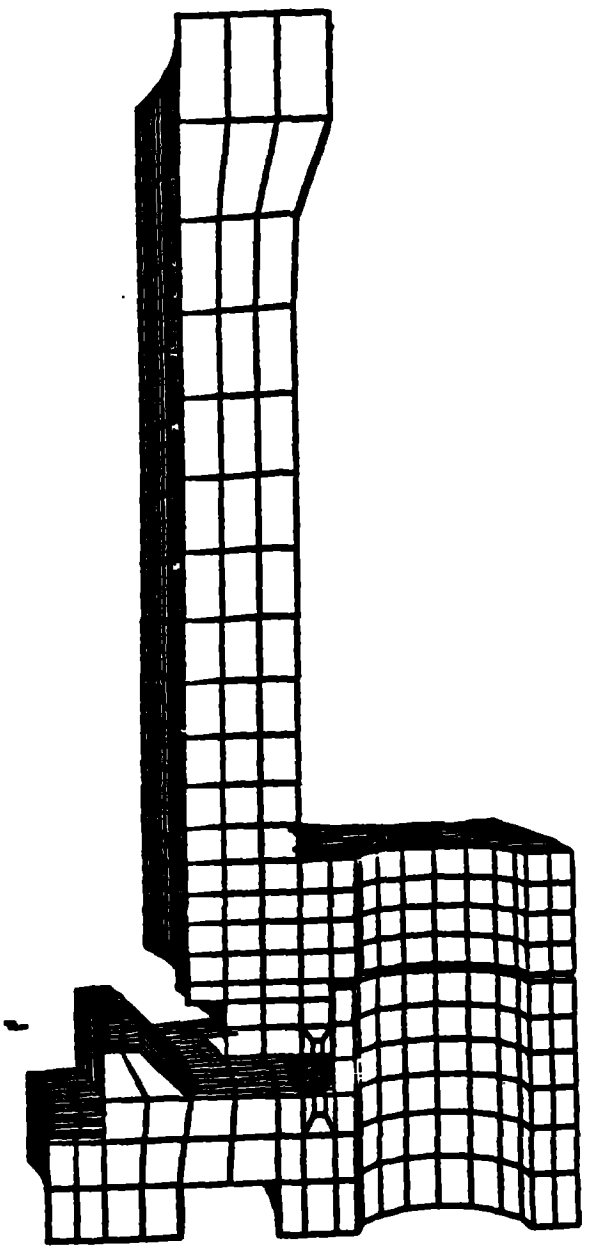

Fig. 20. View of mesh showing bolt hole.

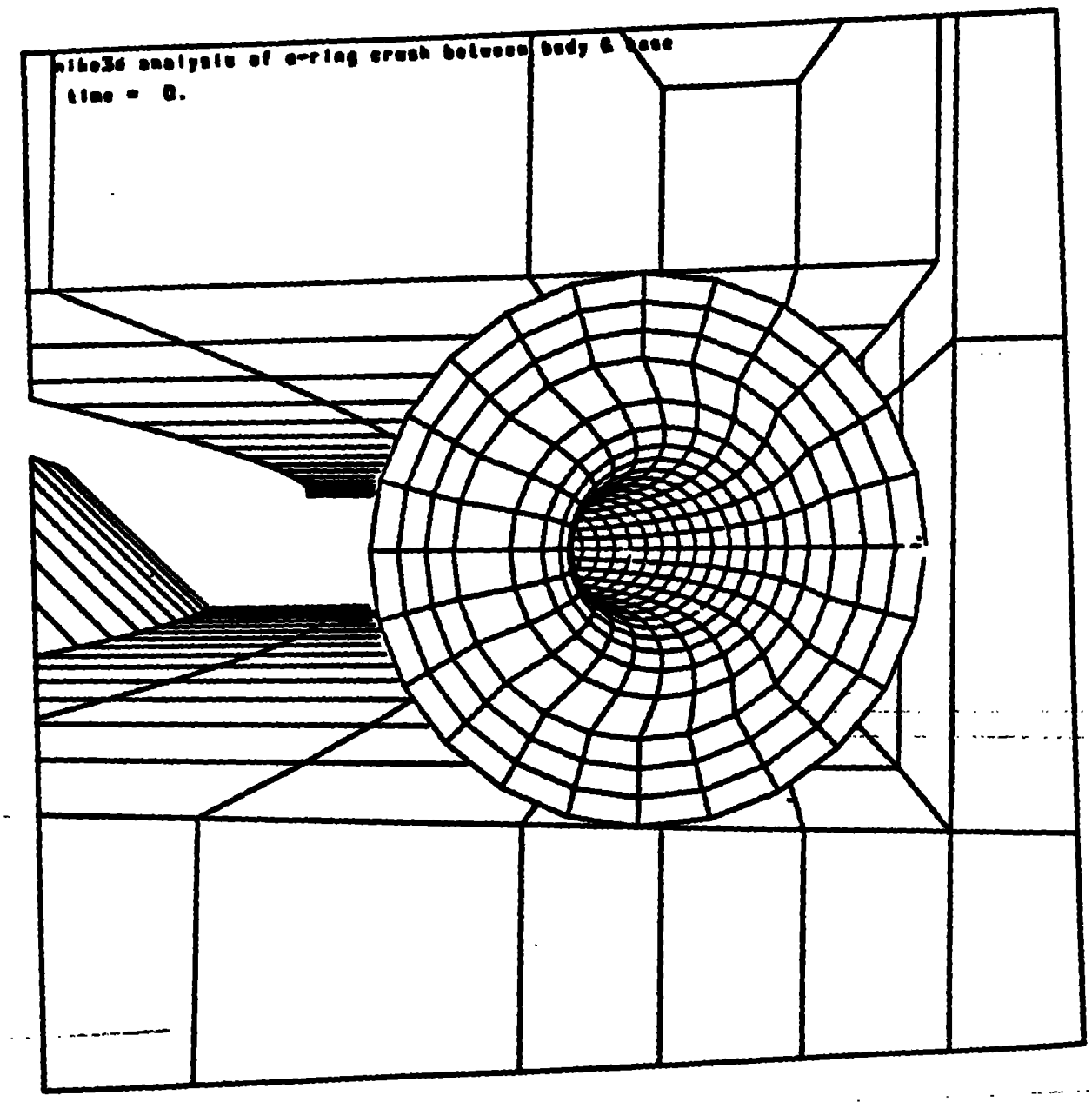

Fig. 21. Close-up view of O-ring at start of calculation.

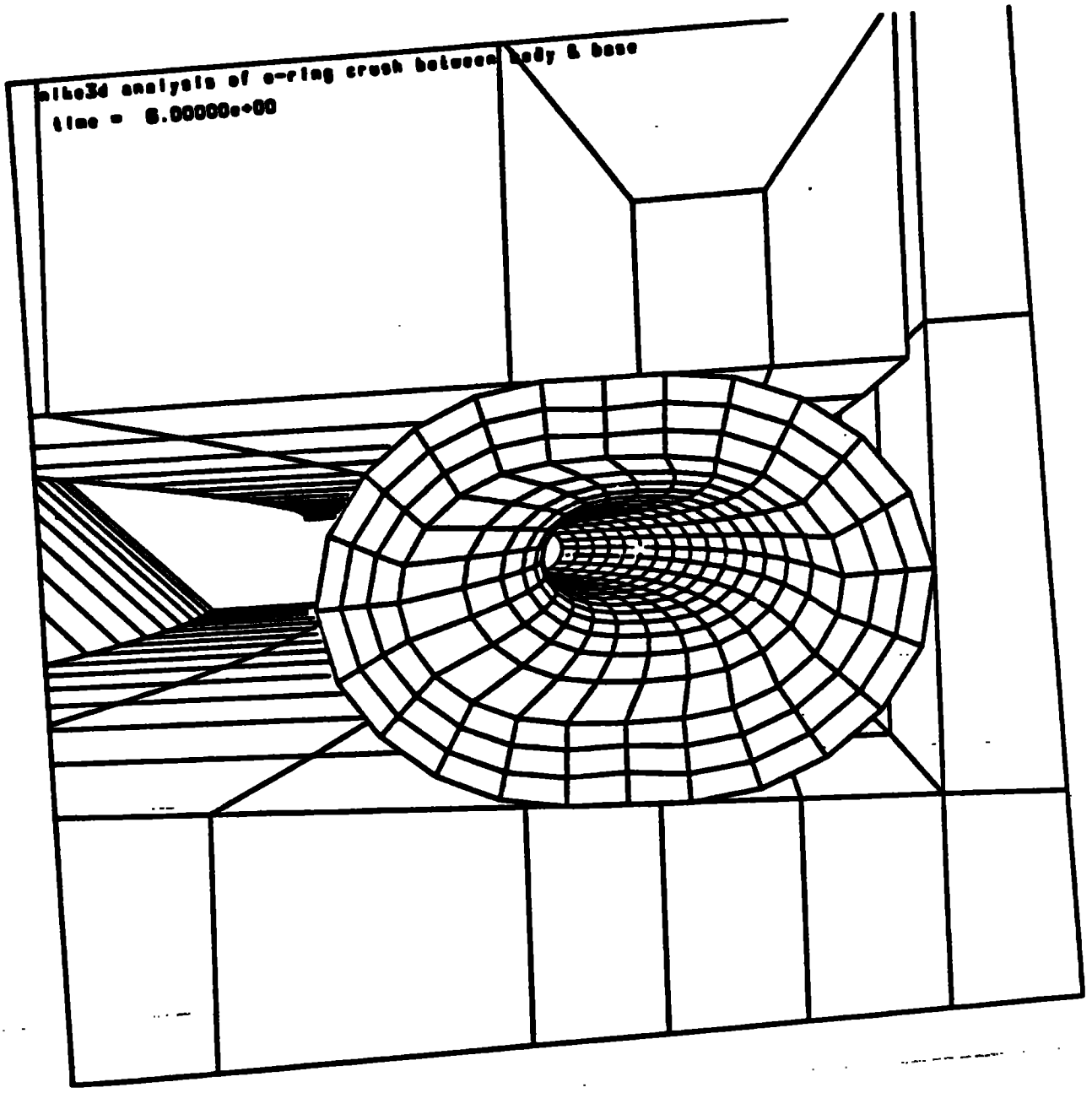

Fig. 22. Deformed O-ring at the completion of the sixth time step.

4. PIPE WHIP

Our final penalty formulation example uses the recently implemented shell elements in NIKE3D.

Current Nuclear Power Plant design regulations require pipes to be designed against pipe whip. It is postulated that in the event of pipe break, the high pressure fluid in the pipe could cause the pipe to swing and impact another pipe. The Nuclear Regulatory Commission has provided multi-year funding to Livermore to study this problem.

A sample problem was developed to test the ability of NIKE3D to solve pipe impact problems. The problem consists of two steel pipes both having a thickness of 0.432 inches, 3.3125, a length of 50 inches. One pipe is oriented horizontally and completely fixed at both ends, and a yield strength of 10^5 psi, and a hardening modulus of 10^5 psi. The other pipe swings about one end in a plane normal to the horizontal pipe. The angular velocity at the time of impact is 50 radians/sec. Shell elements were used in the mesh with one plane of symmetry. Two-hundred steps were used with a termination time of 10 ms. Results from the pipe impact problem are shown in Figs. 23-25. The pipe begins to rebound at approximately 7 ms.

Several experiments on pipe impacts were performed for the Nuclear Regulatory Commission that could provide a basis for verifying the shell impact capability. Efforts were made to obtain the experimental data, but we were denied reasonable access.

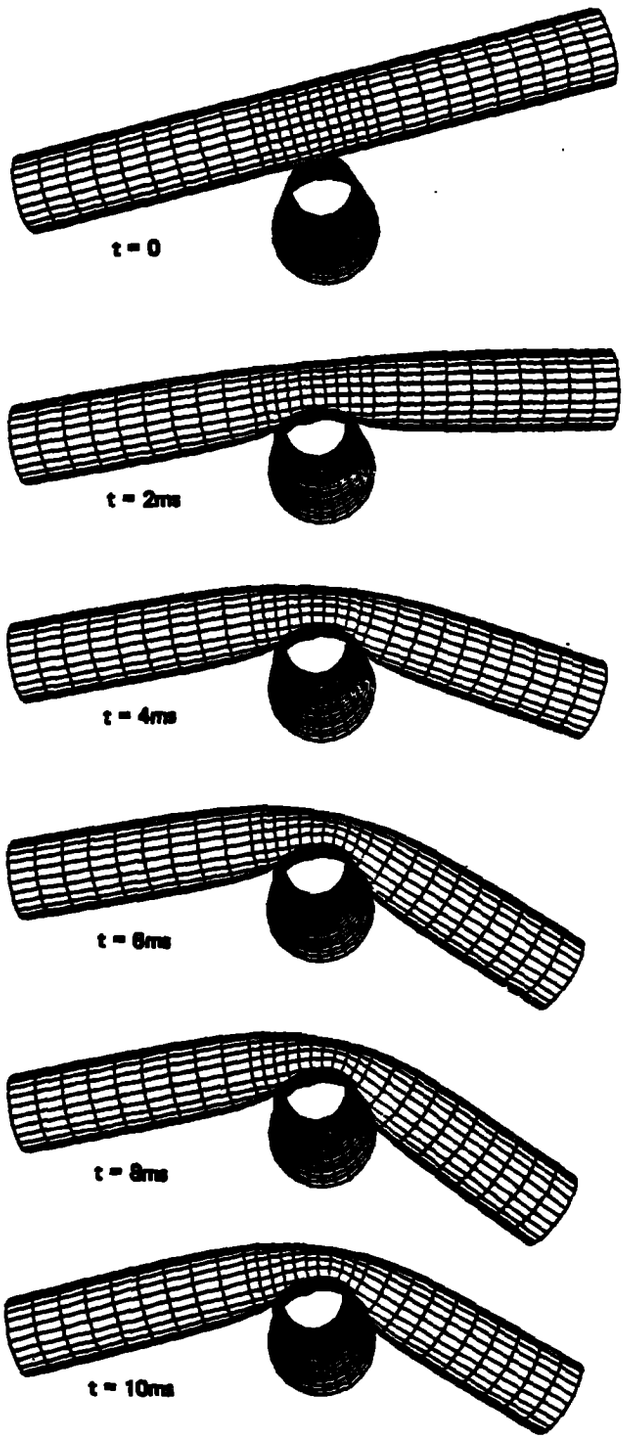

Fig. 23. Sequence of deformed shapes in 2ms intervals.

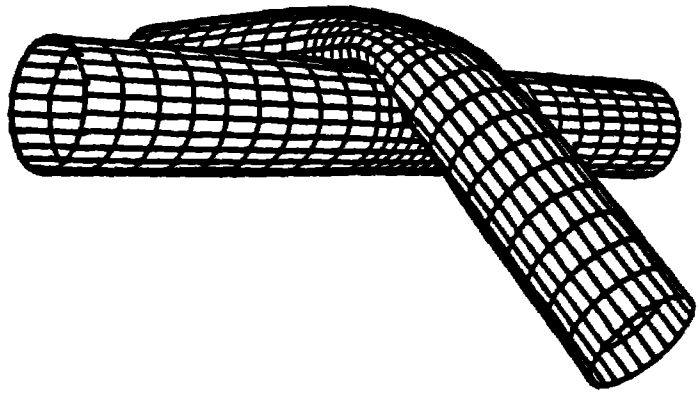

Fig. 24. Rotated view of final configuration.

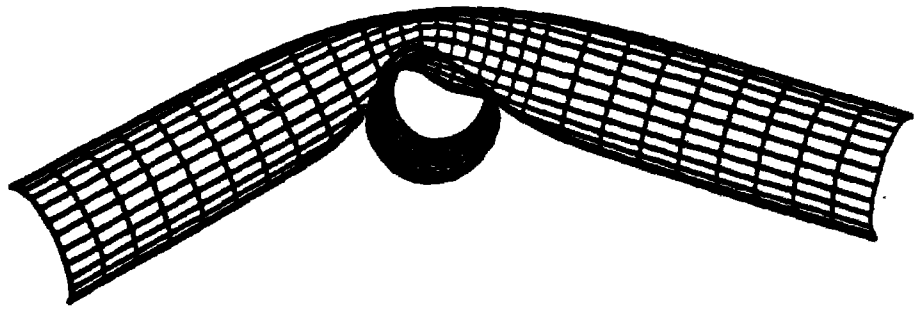

Fig. 25. Deformed cross section.

ACKNOWLEDGEMENTS

This work was performed under the auspices of the U.S. Department of Energy by the Lawrence Livermore National Laboratory under contract number W-7405-Eng-48.

REFERENCES

[1] J. O. Hallquist, NIKE2D: an implicit, finite-deformation, finite-element code for analyzing the static and dynamic response of two-dimensional solids, University of California, Lawrence Livermore National Laboratory, UCRL-52678 (1979).

[2] J. O. Hallquist, NIKE3D: an implicit, finite-deformation, finite element code for analyzing the static and dynamic response of three-dimensional solids, University of California, Lawrence Livermore National Laboratory, UCID-52429 (1978).

[3] J. O. Hallquist, DYNA2D - an explicit finite element and finite difference code for axisymmetric and plane strain calculations, (User's Guide), University of California, Lawrence Livermore National Laboratory, UCRL-52429 (1978).

[4] J. O. Hallquist, User's manuals for DYNA3D and DYNAP (nonlinear dynamic analysis of solids in three dimensions), University of California, Lawrence Livermore National Laboratory, UCID-19156 (1981).

[5] H. Matthies and G. Strang, The solution of nonlinear finite element equations, Int. Journal for Numerical Methods in Engineering, Vol. 14, No. 11, pp. 1613-1626 (1979).

[6] H. F. Walker, Numerical solution of nonlinear equations, University of California, Lawrence Livermore National Laboratory, UCID-18285 (1979).

[7] W. F. Noh, Numerical calculations in hydrodynamic calculations, University of California, Lawrence Livermore National Laboratory, UCRL-52112 (1976).

[8] G. L. Goudreau and J. O. Hallquist, Recent developments in large-scale finite element lagrangian hydrocode technology, J. Comp. Meths. Appl. Eng., 33 (1982) 725-757.

[9] T.J.R. Hughes, R. L. Taylor, and W. Kanoknukulchai, A finite element method for large displacement contact and impact problems, Formulation in Finite Element Analysis, in: Bathe, Oden, and Wunderlich, eds., U.S.-German Symposium on Finite Element Method (1978).

[10] T.J.R. Hughes, R. L. Taylor, I. L. Sackman, A. Curnier, and W. Kanoknubulchai, A finite element method for a class of contact-impact problems, J. Comp. Meths. Appl. Eng., 8 (1976) 233-243.

[11] M. L. Wilkins, Calculation of elastic-plastic flow, in: B. Alder et. al., eds., Methods in Computational Physics, Vol. 3 (Academic Press, New York, 1964) 211-263.

[12] L. D. Bertholf and S. E. Benzley, TOODY II, a computer program for two-dimensional wave propagation, Sandia National Laboratories, SC-RR-68-41 (1968).

[13] G. Maenchen and S. Sack, The TENSOR code, in: B. Alder et. al., eds., Methods in Computational Physics, Vol. 3, (Academic Press, New York, 1964) 181-210.

[14] W. F. Noh, CEL: a time dependent, two-space-dimensional, coupled eulerian-lagrange code, in: B. Olden et. al., eds., Methods in Computational Physics, Vol. 3, (Academic Press, New York, 1964) 117-179.

[15] M. W. Wilkins, Calculation of elastic-plastic flow, University of California, Lawrence Livermore National Laboratory, UCRL-7322, Rev. 1 (1969).

[16] D. B. Tuft and C. S. Godfrey, Computer analysis of a three-dimensional mass focus projectile device, University of California, Lawrence Livermore National Laboratory, UCRL-87678 (1982).